

# Non-covalent interactions that tune the reactivities of the flavins in bifurcating electron transferring flavoprotein

María González-Viegas<sup>a,b</sup>, Rajiv K. Kar<sup>a,d</sup>, Anne-Frances Miller<sup>a,c,\*</sup>  
and Maria-Andrea Mroginski<sup>a,\*</sup>

<sup>a</sup> Department of Chemistry, Technische Universität - Berlin, Berlin, Germany

<sup>b</sup> Department of Physics, Freie Universität Berlin, Berlin, Germany

<sup>c</sup> Department of Chemistry, University of Kentucky, Lexington KY, U.S.A.

Correspondence to A.-F. Miller: [afmill3r2@gmail.com](mailto:afmill3r2@gmail.com) or M.-A. Mroginski:  
[andrea.mroginski@tu-berlin.de](mailto:andrea.mroginski@tu-berlin.de)

Running Title: Interactions that differentiate Bf-ETF's flavins

Key Words: electron transfer, flavoprotein, FAD, hydrogen bond, conformational  
change, electron transfer flavoprotein, electron bifurcation, redox tuning, electron  
density, QM/MM

<sup>d</sup> Current address Jyoti and Bhupat Mehta School of Health Sciences and  
Technology, Indian Institute of Technology Guwahati, Assam, India

## Abstract

Bifurcating electron transferring flavoproteins (Bf-ETFs) tune chemically identical flavins to two contrasting roles. To understand how, we used hybrid quantum mechanical molecular mechanical calculations to characterize non-covalent interactions applied to each flavin by the protein. Our computations replicated the differences between the reactivities of the flavins: the electron transferring flavin (<sup>ET</sup>flavin) was calculated to stabilize anionic semiquinone (ASQ) as needed to execute its single-electron transfers, whereas the Bf flavin (<sup>Bf</sup>flavin) was found to disfavor the ASQ state more than does free flavin and to be less susceptible to reduction. The stability of <sup>ET</sup>flavin ASQ was attributed

1  
2  
3  
4  
5  
6  
7  
8  
9  
10  
11  
12  
13  
14  
15  
16  
17  
18  
19  
20  
21  
22  
23  
24  
25  
26  
27  
28  
29  
30  
31  
32  
33  
34  
35  
36  
37  
38  
39  
40  
41  
42  
43  
44  
45  
46  
47  
48  
49  
50  
51  
52  
53  
54  
55  
56  
57  
58  
59  
60  
61  
62  
63  
64  
65

in part to H-bond donation to the flavin O2 from a nearby His side chain, via comparison of models employing different tautomers of His. This H-bond between O2 and the ET site was uniquely strong in the ASQ state, whereas reduction of <sup>ET</sup>flavin to the anionic hydroquinone (AHQ) was associated with side chain reorientation, backbone displacement and reorganization of its H-bond network including a Tyr from the other domain and subunit of the ETF. The Bf site was less responsive overall, but formation of the <sup>Bf</sup>flavin AHQ allowed a nearby Arg side chain to adopt an alternative rotamer that can H-bond to the <sup>Bf</sup>flavin O4. This would stabilize the anionic <sup>Bf</sup>flavin and rationalize effects of mutation at this position. Thus, our computations provide insights on states and conformations that have not been possible to characterize experimentally, offering explanations for observed residue conservation and raising possibilities that can now be tested.

## 1. Introduction

Electron transferring flavoproteins (ETFs) have been known since the 1950s to shuttle single electron (1e) equivalents among dehydrogenases and the respiratory electron transfer chain of mitochondria and aerobic bacteria [1-3]. This activity is mediated by a flavin adenine dinucleotide (FAD) bound in a domain ('head' or 'shuttle'), that is found in one of two orientations relative to a 'base' composed of domains I and III, in crystal structures [4]. Naming of ETFs' two subunits and the domains is provided in Figure 1.

In the 1970s, the first report appeared of an ETF containing a second FAD [5], replacing what now appears to be a vestigial adenosine monophosphate [6-8]. It is now apparent that diverse anaerobes employ such bifurcating ETFs (Bf-ETFs) to generate more strongly reducing electron carriers (with lower reduction midpoint potentials,  $E^\circ$ s) based on abundant but only modestly reducing nicotinamide adenine dinucleotide (NADH) [9,10].

'Bifurcation', or more accurately electron transfer bifurcation, captures excess energy released from a favorable electron transfer (ET) to higher  $E^\circ$ , by using it to drive an unfavorable transfer [9]. The resulting reduced flavodoxin and ferredoxin provide reducing equivalents needed for demanding reactions including nitrogen fixation and carbon fixation [11-13]. In brief, a pair of electrons is acquired from NADH by a flavin dubbed the 'bifurcating flavin' ( $B^f$ flavin) because it passes each of the two electrons to separate acceptors. One electron undergoes exergonic electron transfer via the electron transferring flavin ( $E^T$ flavin), thereby paying for endergonic ET of the second electron to a low- $E^\circ$  acceptor (Figure 1). To prevent both of NADH's electrons from exploiting the exergonic path, it is critical that the  $E^T$ flavin only accept electrons one at a time. In contrast, the  $B^f$ flavin needs to acquire electrons in pairs from NADH. Thus, it might seem surprising that nature has adopted the use of flavins for both roles.

A conformational change is believed to act as a gate, separating the  $E^T$ flavin from the  $B^f$ flavin after one electron has been transferred, and thereby enforcing transfer of the other electron to the other acceptor [14,15]. The two conformations seen in crystal structures reveal an  $80^\circ$  rigid-body rotation of the shuttle domain that carries the  $E^T$ flavin, removing it from near the  $B^f$ flavin [16,17] to a position more than 35 Å away and interacting instead with the high- $E^\circ$  acceptor partner protein [4,14,15,18,19]. It remains unclear how this domain movement is coupled to catalytic events, and what local perturbations trigger it. However, we note that the high  $E^\circ$  determined for reduction of the  $E^T$ flavin from OX to

1 ASQ ( $E^{\circ}_{OX/ASQ}$ ), suggests that  $^{ET}$ flavin will be ASQ in resting enzyme, and therefore only  
2 capable of accepting one more electron. Thus, the redox tuning applied by the protein  
3 environment appears to make the  $^{ET}$ flavin into a 1e acceptor [6,20,21].  
4

5 Indeed, we argue that the extreme chemical versatility of flavins has made them  
6 invaluable cofactors over the course of evolution, as different proteins can be evolved to  
7 emphasize different aspects of the flavin's repertoire by surrounding it with amino acid  
8 residues that modify the flavin electronics and accessibility in different ways [22]. Thus,  
9 biosynthesis of this one cofactor enables cells to satisfy many catalytic needs [23]. At  
10 issue here, the isoalloxazine core of the flavin is poised between 1e and 2e reactivity by  
11 its two 1e  $E^{\circ}$ s that are weakly crossed [9,24], resulting in predominantly 2e reduction  
12 from the oxidized state (OX) to the 2e reduced hydroquinone (HQ), but with a  
13 thermodynamically accessible semiquinone (SQ) state that is populated to approximately  
14 1% at neutral pH [24]. Thus, a protein site able to make relatively modest changes to the  
15 relative energies of the OX, SQ and HQ states can shift the reactivity of the flavin between  
16 1e and 2e transfers. Furthermore, both the SQ and HQ states have physiologically  
17 accessible  $pK_{as}$ , of 8.5 and 6.8, respectively [24,25]. Consequently, proteins can modulate  
18 local electrostatics to (dis)favor the anionic SQ (ASQ) or anionic HQ (AHQ) [26], or they  
19 can modulate the favorability of proton transfer coupled to ET. Further interventions are  
20 achieved via orchestrated changes of the local dielectric that can alter the energy  
21 associated with a given charge [27]. Steric interactions producing distortions  
22 characteristic of more reduced states are also expected to raise the flavin  $E^{\circ}$ s [28,29].  
23 Additionally, the flavin  $\pi$  system incorporates several functionalities that engage in  
24 hydrogen bonds (H-bonds). These provide additional mechanisms by which proteins can  
25 tune the reactivity of flavins (Scheme 1). Vibrational spectroscopy reveals that the flavins'  
26 two carbonyl O atoms respond to H-bonding, and NMR reveals changes in local electron  
27 density distribution as a result of H-bonds to the O and N atoms [30-33].  
28

29 ETFs appear to employ several of the above features to tune the relative stability of  
30 the  $^{ET}$ flavin's ASQ [34-36]. A positively charged Arg or Lys adjacent to the  $^{ET}$ flavin is  
31 conserved in of 98% of Bf-ETFs, and has been shown to stabilize the ASQ and impede  
32 formation of the AHQ [34-37]. Bf-ETFs also conserve a Thr or a Ser near the N5 of the  
33  $^{ET}$ flavin and substitution of this residue affects the  $E^{\circ}$ s [37]. Additionally, a His near  
34  $^{ET}$ flavin's O2 is conserved in 90% of Bf-ETFs but has not been as well characterized in  
35 the literature (statistics are based on an alignment of 228 Bf-ETF sequences [38]). The Bf  
36 site also possesses a 99% conserved Arg (otherwise Lys). Unfortunately, its substitution  
37  
38  
39  
40  
41  
42  
43  
44  
45  
46  
47  
48  
49  
50  
51  
52  
53  
54  
55  
56  
57  
58  
59  
60  
61  
62  
63  
64  
65

1 destabilizes the protein and abrogates flavin binding. Therefore, little is known about how  
2 it may affect the reactivity of the flavin [34]. Moreover, because the ASQ state of <sup>Bf</sup>flavin  
3 does not normally accumulate in high-quality ETF preparations, it is not possible to study  
4 it experimentally to learn how the protein destabilizes it. Thus, computational approaches  
5 can fill a critical knowledge gap, elucidating mechanisms of tuning applicable to the  
6 <sup>Bf</sup>flavin, while using the more accessible <sup>ET</sup>flavin as a control for which computations can  
7 be validated by experiments [6].  
8  
9  
10  
11  
12  
13  
14  
15

16 **Figure 1** The two FAD-binding sites in the context of the Bf-ETF ribbon structure in the  
17 'closed' conformation, based on the crystal structure of *Afe*ETF [39]. An 80° rotation of the  
18 shuttle domain produces the 'open' conformation (SI Figure S1 [14,15]). The larger EtfA  
19 polypeptide is in light grey and the smaller EtfB polypeptide is in dark grey. Flavin head groups  
20 are in heavy ball-and-stick cartoons with the balance of the FAD and residues of special interest  
21 shown as sticks. Residues are numbered according to *Afe*ETF and those derived from EtfB bear  
22 an apostrophe. C atoms are colored teal for the <sup>ET</sup>flavin and purple for the <sup>Bf</sup>flavin. All other  
23 atoms are colored according to the CPK convention. Heavy arrows indicate electron transfers  
24 involved in bifurcation.  
25  
26  
27  
28  
29  
30  
31  
32  
33  
34  
35

36 **Scheme 1:** Flavin oxidation states discussed in this study and numbering of key positions in  
37 italics (all viewed from *si* face, numbering shown for OX only). Full numbering is provided in  
38 Scheme S1. In the text, H5 denotes the H atom whereas N5 denotes the N atom, both at the 5  
39 position. R = ribityl adenosine diphosphate for FAD, truncated to -CH<sub>3</sub> in quantum mechanical  
40 (QM) calculations. States shown are OX, oxidized; ASQ, anionic semiquinone (1e reduced);  
41 AHQ, anionic hydroquinone (2e reduced); AHQ<sub>H1</sub>, anionic hydroquinone protonated at N1  
42 instead of N5 (2e reduced).  
43  
44  
45  
46  
47  
48  
49  
50  
51  
52

## 53 2. Results

54 We begin by validating our computational approach (section 2.1), then provide a  
55 comparative overview of interactions observed in each of the two sites (2.2), before  
56 describing striking electrostatic differences between them (2.3). Section 2.4's  
57 examination of H-bonding in the ET site identifies interplay between H-bonding at <sup>ET</sup>O2,  
58  
59  
60  
61  
62  
63  
64  
65

1 formation of <sup>ET</sup>ASQ and the protonation state of <sup>ET</sup>N5, that enable a conserved His at  
2 position 290 to influence reactivity at <sup>ET</sup>N5. Whereas the crystallographic Bf site seems  
3 considerably less responsive to flavin oxidation state than the ET site, based on our  
4 models obtained by energy-minimization (section 2.5) a model incorporating an  
5 alternative rotamer of R146 raises interesting new possibilities (section 2.6), and suggests  
6 a basis for the high conservation of this residue.  
7  
8  
9

### 10 2.1 Validation: Computational replication of contrasting flavin reactivities.

11 Before using our models to *explain* the contrasting reactivities of the two flavins, we  
12 tested whether they succeed in *reproducing* the differences. In experiments, the ET site  
13 stabilizes <sup>ET</sup>ASQ, populating this state to 90% during stepwise reductions [64]. In  
14 contrast, free flavin only accumulates 1 % of the population as ASQ whereas  $\geq 99\%$   
15 undergoes 2e reduction directly from OX to AHQ [24]. Thus, a favorable ASQ state,  
16 specifically in the ET site, is a critical test of whether our models correctly describe this  
17 site. The ET site also makes bound flavin more amenable to reduction than free flavin,  
18 whereas the Bf site has the opposite effect [6,20,21,64], so a test of our Bf site models is  
19 that they should disfavor flavin reduction.  
20  
21  
22  
23  
24  
25  
26  
27  
28

29 Our models succeed on both criteria. Based on Gibbs free energy differences (Table  
30 1), formation of ASQ from OX is favorable in the ET site, only. The contrasting computed  
31 energy differences clearly stem from the protein, as the two sites produced deviations in  
32 opposing directions from the value for gas-phase flavin. Second, formation of AHQ was  
33 calculated to be less favorable in the Bf site than in either the ET site or the gas phase,  
34 validating our models of that site as well. Although qualitative, these successes are  
35 impressive considering the many aspects of protein environments that can contribute to  
36 flavin reactivity (see Introduction), in conjunction with the computational parsimony  
37 required to permit the desired characterizations of the numerous states believed to  
38 contribute to reactivity.  
39  
40  
41  
42  
43  
44  
45  
46  
47

48 >>Table 1 belongs here<<  
49  
50  
51  
52

53 Because they replicate the different reactivities of the two flavins, our computations  
54 provide a basis for evaluation of the roles played by different aspects of the protein  
55 environment. Here we have considered local electrostatics, geometry imposed by the  
56  
57  
58  
59  
60  
61  
62  
63  
64  
65

1 protein, and H-bonds. Such factorization is difficult in experiments, where residue  
2 substitutions tend to change all three contributions at once.

### 3 4 2.2 Overview of the sites' geometries and protein-flavin interactions

5 Our computations reveal interplay between each flavin and protein residues nearby, as  
6 summarized in Scheme 2. H-bonding with flavin positions N3 and O4 was found to be  
7 mainly with protein backbone carbonyl (=O) and amide (NH) groups, and therefore could  
8 be coupled to higher-order structure. However H-bonds to flavin O2 were also provided  
9 by side chains or a water molecule, which can be more mobile. H-bond donation to flavin  
10 N5 was also via amino acid side chains in both sites, which is significant because the 5  
11 position is converted from a H-bond *acceptor* to a H-bond *donor* upon acquisition of a  
12 proton as part of reduction to form AHQ (Scheme 1). Thus, ETF's presentation of side  
13 chains to that position obviates a need for the backbone reorientation seen in flavodoxin  
14 [65]. In both sites, reorientation of the side chain interacting at N5 enabled the protein to  
15 accept a H-bond from the flavin AHQ, where it had donated one to OX and ASQ (sections  
16 2.4 and 2.5).  
17  
18  
19  
20  
21  
22  
23  
24  
25  
26  
27  
28  
29  
30  
31  
32

33 Scheme 2. Residues that interact with each of the <sup>ET</sup>flavin and the <sup>Bf</sup>flavin. Flavins are  
34 viewed from the *si* face and portrayed in their OX states. Weak interactions or interactions  
35 specific to particular oxidation states are in parentheses, see text for details. T94' (in purple)  
36 resides in EtfB monomer whereas all other residues specified in this scheme derive from EtfA.  
37 The H-bond to N1 of the <sup>ET</sup>flavin derives from the <sup>ET</sup>FAD's own ribityl chain [66]. Amino acid  
38 side chain atoms bear Greek specifiers whereas the backbone amide N and H and the backbone  
39 carbonyl O do not. This convention will be used throughout.  
40  
41  
42  
43  
44  
45

46 Reduction of <sup>ET</sup>flavin to <sup>ET</sup>AHQ caused the side chains of S270 and Q266 to reorient,  
47 reversing the polarities of their interactions with the <sup>ET</sup>flavin. In addition, a segment of  
48 backbone at G271 relinquished its H-bond to <sup>ET</sup>O4 and moved away by 1 Å (Figure 2A).  
49 Thus, the protein constituents of our computed ET site are conformationally responsive  
50 to the oxidation state of <sup>ET</sup>flavin and not frozen in the <sup>ET</sup>OX crystal structure. Our  
51 computations thus suggest that the ET site supports facile <sup>ET</sup>flavin reduction via provision  
52 of a highly fluid or adaptive network of H-bonds from mobile side chains and backbone  
53 loops.  
54  
55  
56  
57  
58  
59  
60  
61  
62  
63  
64  
65

1  
2  
3 **Figure 2:** Overlay of  ${}^{\text{ET}}\text{OX}_\delta$ ,  ${}^{\text{ET}}\text{ASQ}_\delta$ ,  ${}^{\text{ET}}\text{AHQ}_\delta$ . The  ${}^{\text{ET}}$ flavin is viewed from the *si* face (A)  
4 and from the xylene ring end (B) with the energy-minimized structure of  ${}^{\text{ET}}\text{OX}$  in brown, that of  
5  ${}^{\text{ET}}\text{ASQ}$  in light green and that of  ${}^{\text{ET}}\text{AHQ}$  in darker teal. The lowest-energy structures are shown,  
6 corresponding to the second energy minimum of  ${}^{\text{ET}}\text{AHQ}$  as described below. Panel A shows the  
7 displacement of backbone near G271 upon reduction to the  ${}^{\text{ET}}\text{AHQ}$  state (lower left of panel).  
8 The same displacement is evident in the lower right of panel B in the orientation of S270's  
9 backbone O.

### 16 2.3 Effect of protein electrostatics on distribution of electron density in the flavins

17 Electrostatic stabilization of the different flavin oxidation states by each of the protein  
18 sites was assessed via computation of Natural Bond Order electron densities (NBO [67]).  
19 Figure 3 shows how the NBO densities deviated from what occurs if the flavin is  
20 considered in gas-phase but frozen in the geometries produced by the corresponding  
21 protein site.  
22  
23  
24  
25  
26  
27  
28  
29  
30

31 **Figure 3:** Flavin ring structures with positions color-coded by differences in the NBO  
32 partial charges produced by the protein electrostatic environment. The flavin geometries were  
33 held constant as optimized in the protein QM/MM, and the protein environment was provided in  
34 the form of the partial charges of the protein atoms. To emphasize the effect of protein  
35 electrostatics, differences plotted are 'in presence of protein charges' minus 'in absence of  
36 protein charges' with the same flavin geometry (a.k.a. 'frozen gas phase'). Hydrogen charges  
37 were added to those of the heavy atoms to which they are bound. Partial charge values are  
38 shown in SI Tables S2, S3, S4 and S5.  
39  
40  
41  
42  
43  
44  
45

46 All oxidation states of the  ${}^{\text{Bf}}$ flavin showed greater charge displacements, compared to  
47 the  ${}^{\text{ET}}$ flavin. In  ${}^{\text{Bf}}$ flavin, position  ${}^{\text{Bf}}\text{N5}$  especially, followed by  ${}^{\text{Bf}}\text{O4}$ ,  ${}^{\text{Bf}}\text{O2}$ ,  ${}^{\text{Bf}}\text{C6}$  and  ${}^{\text{Bf}}\text{C9}$   
48 differed from free flavin with the same geometry. It is fascinating that (1) two  
49 unsubstituted aromatic Cs were significantly affected ( ${}^{\text{Bf}}\text{C6}$  and  ${}^{\text{Bf}}\text{C9}$ ), (2) the largest  
50 effects were on electronegative atoms but of these,  ${}^{\text{Bf}}\text{N1}$  and  ${}^{\text{Bf}}\text{O2}$  were net electron-  
51 depleted while  ${}^{\text{Bf}}\text{O4}$  and  ${}^{\text{Bf}}\text{N5}$  were enriched. A pattern that emerges is that atoms along  
52 the 'top' edge as displayed ( ${}^{\text{Bf}}\text{C9}$ ,  ${}^{\text{Bf}}\text{C10}$ ,  ${}^{\text{Bf}}\text{C1}'$ ,  ${}^{\text{Bf}}\text{N1}$ ,  ${}^{\text{Bf}}\text{O2}$ ) were rendered electron  
53 deficient by the Bf site, but not the ET site. We speculate that this reflects electrostatic  
54  
55  
56  
57  
58  
59  
60  
61  
62  
63  
64  
65



1 repulsion by the pyrophosphate of the <sup>Bf</sup>FAD because the kinked conformation of the  
2 <sup>Bf</sup>FAD's ribose places the phosphates less than 6 Å from the 'top' edge of the <sup>Bf</sup>flavin  
3 (Figure 1), whereas, the <sup>ET</sup>FAD is more extended.  
4

5 The ET site produced completely different effects on NBO density, barely perturbing  
6 excess electron density distribution in <sup>ET</sup>OX, compared to gas phase. This is consistent  
7 with <sup>ET</sup>flavin's greater solvent accessibility in *Afe*ETF [34]. However in <sup>ET</sup>ASQ, the <sup>ET</sup>N1  
8 position bore much more excess electron density, as did <sup>ET</sup>O2. Among the heteroatoms,  
9 the only position to bear more positive charge relative to that seen for gas-phase flavin  
10 was <sup>ET</sup>N3H (sum of NBO charges of <sup>ET</sup>N3 and <sup>ET</sup>H3), in further contrast with <sup>Bf</sup>flavin.  
11 This concentration of negative charge on electronegative <sup>ET</sup>N1 and <sup>ET</sup>O2 was specific to  
12 the <sup>ET</sup>ASQ state and is chemically favorable, suggesting a basis for the unique stability of  
13 <sup>ET</sup>ASQ. However, it is not easy to explain based on charged residues nearby. The only  
14 charged side chain within 7 Å of <sup>ET</sup>flavin is that of R253, and its guanidinium  
15 functionality is closer to the flavin xylene ring than to <sup>ET</sup>O2 and <sup>ET</sup>N1.  
16  
17

#### 18 2.4 Interactions in the ET site

19 To understand migration of electron density to <sup>ET</sup>O2, we investigated H-bonds nearby.  
20 His290 is conserved in 90% of Bf-ETF sequences, so we tested the possible significance  
21 of a H-bond by modeling H290 in two tautomers. The δ-tautomer bearing an H on the δN  
22 could donate a H-bond to <sup>ET</sup>O2 but the ε-tautomer bearing an H on the εN instead could  
23 not, based on the energy minimized structures (Figure 4). Indeed, Figure 3 shows that  
24 strong excess electron density on <sup>ET</sup>O2 was specific to the δ tautomer, indicating that H-  
25 bond donation from H290 is responsible.  
26

27 If a H-bond is to tune an  $E^\circ$  of <sup>ET</sup>flavin, it must change the energy of one oxidation  
28 state more than that of the other state. This is a result of the direct proportionality between  
29  $E^\circ$  and the free energy change upon reduction, where  $n$  is the number of electron  
30 equivalents acquired and  $F$  is Faraday's constant. For the example of reduction of OX to  
31 ASQ,  $E^\circ_{OX/ASQ} = -(G^\circ_{ASQ} - G^\circ_{OX})/nF$  and  $n=1$ . If a H-bond lowers the free energy  
32 of the ASQ state more than the free energy of the OX state, then the quantity inside the  
33 parentheses becomes more negative and the right side of the equation becomes more  
34 positive ( $F$  is positive). Thus, the new  $E^\circ_{OX/ASQ(Hbd)}$  modified by H-bonding becomes  
35 more positive. This is illustrated in supporting Figure S2. Because a stronger (shorter) H-  
36 bond lowers a state's energy more than a weaker (longer) one, the foregoing example  
37 would correspond to a shorter H-bond in the ASQ state than in the OX state.  
38  
39  
40  
41  
42  
43  
44  
45  
46  
47  
48  
49  
50  
51  
52  
53  
54  
55  
56  
57  
58  
59  
60  
61  
62  
63  
64  
65

1 H-bond strengths were therefore assessed, via the proxy of their lengths, and compared  
2 for all three observed oxidation states (Tables S6, S7, S8). In the ET site, some H-bond  
3 lengths were relatively invariant (changes  $\leq 0.2$  Å in donor-acceptor distances [68]).  
4 However four underwent qualitative change, being engaged only in certain oxidation  
5 state(s) (Table S8). These included the H-bond between  $^{ET}O2$  and H290 whose H moves  
6 into H-bonding position between the two heavy atoms only in the  $^{ET}ASQ$  state (Figure  
7 4B). Additional responsive H-bonds were from backbone to  $^{ET}O4$  (Figure 4A), a weak H-  
8 bond from the side chain of Q266 to  $^{ET}O4$  that is exclusive to the AHQ state (Figure 4C),  
9 and the interaction between  $^{ET}N5$  and the side chain of S270 that reverses polarity upon  
10 formation of  $^{ET}AHQ$  (with acquisition of the  $^{ET}H5$  proton, Figure 4A).

11 H-bonds involving backbone are of particular interest, because repositioning of  
12 backbone could trigger changes in the protein secondary and higher-order structure. In  
13 the ET site, the backbone HN of G271 H-bonded to  $^{ET}O4$  in  $^{ET}OX$  and  $^{ET}ASQ$ , but was  
14 released upon formation of  $^{ET}AHQ$ . The  $^{ET}O4$  - N distance increased from 3.0 to 3.9 Å in  
15  $^{ET}AHQ_{\delta}$ , and from 3.1 Å to 4.0 Å in  $^{ET}AHQ_{\epsilon}$ . Detachment of G271 was coupled to  
16 rotation of the sidechain of Q266 which changed from being a recipient from  $^{ET}H3$  of  
17  $^{ET}OX$  or  $^{ET}ASQ$ , to being a H-bond donor to  $^{ET}O4$  of  $^{ET}AHQ$  (see Figure 2). Although  
18 these interactions with  $^{ET}$ flavin were weak, the unambiguous rotation of Q266's side chain  
19 confirmed distinct and adaptive interactions in the different oxidation states.

20  
21  
22  
23  
24  
25  
26  
27  
28  
29  
30  
31  
32  
33  
34  
35  
36  
37  
38 **Figure 4:** Interactions responsive to  $^{ET}$ flavin's oxidation state. (A) H-bond network for  
39  $^{ET}OX_{\delta}$  viewed from the *si* face (top) or edge-on with N5 in front and the ribose-bearing edge  
40 behind. (B) Tautomers of H290 present in  $^{ET}OX_{\epsilon}$  (top, yellow C atoms in flavin) and  $^{ET}OX_{\delta}$   
41 (below, teal C atoms for flavin). (C) Conformations of Q266 produced by energy minimization  
42 of  $^{ET}OX$  or  $^{ET}ASQ$  (top) vs. the conformation of Q266 produced by energy minimization of  
43  $^{ET}AHQ$  (yellow  $^{ET}flavin_{\epsilon}$  and teal  $^{ET}flavin_{\delta}$ ).

44  
45  
46  
47  
48  
49 Similar redox-coupled rotations of H-bonding Gln side chains have been noted in other  
50 flavoproteins, such as BLUF [69,70]. Since gas-phase calculations indicated that the  
51 charge density at  $^{ET}N3$  changes relatively little upon reduction of the flavin, but that  $^{ET}O4$   
52 becomes considerably more negative, especially upon reduction to  $^{ET}AHQ$  (Figure S3),  
53 we speculate that this change corresponds to recruitment of the Q266 amide by  $^{ET}O4$ . The  
54  
55  
56  
57  
58  
59  
60  
61  
62  
63  
64  
65

1 effect would be to stabilize  ${}^{\text{ET}}\text{AHQ}$ , consistent with the  ${}^{\text{ET}}$ flavin's relatively high  $E^{\circ}_{\text{OX/AHQ}}$   
2 [34].

3 Although H-bond donation mediated by  ${}^{\text{ET}}\text{H5}$  is possible only in the  ${}^{\text{ET}}\text{AHQ}$  state,  
4 acceptance at  ${}^{\text{ET}}\text{N5}$  can be compared among all three oxidation states. By comparing an  
5 H-bonds' lengths across states we can determine whether the H-bond is stronger (more  
6 stabilizing) in one state than the other. An H-bond that is stronger in the reduced state  
7 will favor reduction and raise  $E^{\circ}$  (also see supporting Figure S2). We employed an  
8 expanded QM region including S270's side chain in relaxed energy scans of the distance  
9 between  ${}^{\text{ET}}\text{N5}$  and the H-bonding H, to compare energy profiles in each oxidation state.  
10 In the absence of a H-bond to  ${}^{\text{ET}}\text{O2}$ , the energy landscapes were dominated by a single  
11 geometry with a well-defined but long optimal H-to- ${}^{\text{ET}}\text{N5}$  distance (yellow curves in  
12 Figure 5, optimal distance values are provided above each profile for the system with the  
13  $\delta$  tautomer of H290). Energies associated with H-to- ${}^{\text{ET}}\text{N5}$  distances exceeding 2.1 Å are  
14 likely small [61,71], and were not considered to constitute a H-bond [54]. For reference,  
15 distances on the order of  $1.7 \pm 0.1$  Å were obtained between the H-bonding H and the  
16 accepting O atom in work on rhodopsin [61]. Interestingly, several profiles revealed that  
17 more than one configuration of interactions can produce a stable minimum. These  
18 occurred when  ${}^{\text{ET}}\text{N5}$  was protonated (Figure 5B) or when  ${}^{\text{ET}}\text{O2}$  received a H-bond, despite  
19 the spatial separation of these two interactions. The associated structures revealed a  
20 network of interacting residues surrounding  ${}^{\text{ET}}\text{N5}$  and  ${}^{\text{ET}}\text{H5}$  (SI Figure S4). Thus, the  
21 observed stabilization is the result of numerous weak interactions rather than a single  
22 strong one.  
23  
24  
25  
26  
27  
28  
29  
30  
31  
32  
33  
34  
35  
36  
37  
38  
39  
40  
41  
42

43 **Figure 5:** Relaxed energy scans of the interaction with  ${}^{\text{ET}}\text{N5}$  in the different states of the ET  
44 site. (A) The H-to-N5 distance from S270's H $\gamma$  to the  ${}^{\text{ET}}$ flavin that was scanned, shown in the  
45 presence of each of the H290 tautomers tested. (B) Scans of the H $\gamma$ -to- ${}^{\text{ET}}\text{N5}$  distance between  
46 S270 and  ${}^{\text{ET}}\text{N5}$ . Some of the systems displayed a second energy minimum at longer H $\gamma$ -to- ${}^{\text{ET}}\text{N5}$   
47 distance. (C)  ${}^{\text{ET}}$ flavin and S270 geometries for the second energy minima. The energy difference  
48 between  ${}^{\text{ET}}\text{OX}_{\epsilon}$  and  ${}^{\text{ET}}\text{OX}_{\delta}$  was  $\epsilon - \delta = 7.8$  kcal/mol, for  ${}^{\text{ET}}\text{ASQ}_{\epsilon}$  and  ${}^{\text{ET}}\text{ASQ}_{\delta}$  it was 23.4 kcal/mol,  
49 and  ${}^{\text{ET}}\text{AHQ}_{\epsilon}$  and  ${}^{\text{ET}}\text{AHQ}_{\delta} = 16$  kcal/mol. Additionally, the energy differences between first and  
50 second local minima (first minimum minus second minimum) were: -0.4 kcal/mol ( ${}^{\text{ET}}\text{OX}_{\delta}$ ), -  
51 5.5kcal/mol ( ${}^{\text{ET}}\text{ASQ}_{\delta}$ ), **1.1 kcal/mol** ( ${}^{\text{ET}}\text{AHQ}_{\delta}$ ) and **0.5 kcal/mol** ( ${}^{\text{ET}}\text{AHQ}_{\epsilon}$ ). Positive energy  
52 differences indicate that the newly discovered local energy minimum is more stable than the  
53  
54  
55  
56  
57  
58  
59  
60  
61  
62  
63  
64  
65

1 starting geometry (values in bold), and therefore that any H-bond to <sup>ET</sup>AHQ from S270 appears  
2 to dissociate in the <sup>ET</sup>AHQ state, confirming expected behavior.  
3

4 We also characterized H-bonding at <sup>ET</sup>O2 because receipt of a H-bond at <sup>ET</sup>O2 enabled  
5 stable second minima, similar to acquisition of a proton at <sup>ET</sup>N5 (Figure 5B). To test for  
6 participation in redox tuning, we profiled H-bond acceptance strength vs. oxidation state  
7 by scanning along <sup>ET</sup>O2's H-bond in the three oxidation states with the  $\delta$  tautomer of  
8 H290 (Figure 6). In the event of negative cooperativity between protonation at <sup>ET</sup>N5 and  
9 <sup>ET</sup>O2 H-bond acceptance, we expect a longer optimal H-bond to <sup>ET</sup>O2 in <sup>ET</sup>AHQ $\delta$   
10 (protonated at <sup>ET</sup>N5) than in <sup>ET</sup>ASQ $\delta$ , despite their identical total charges. Computations  
11 confirmed this, as well as a broader energy landscape in the <sup>ET</sup>AHQ $\delta$  state where  
12 protonation of <sup>ET</sup>N5 limits electron density migration to <sup>ET</sup>O2 (Figure 3).  
13  
14  
15  
16  
17  
18  
19  
20

21 In contrast, the tighter potential well for the <sup>ET</sup>ASQ $\delta$  state (Figure 6B) reinforces the  
22 evidence of charge distribution and the lower energy of <sup>ET</sup>ASQ $\delta$  vs <sup>ET</sup>ASQ $\epsilon$  that there is a  
23 favorable synergy between the <sup>ET</sup>ASQ state and H-bonding to <sup>ET</sup>O2. The shorter O2 -  
24 HisH $\delta$  distance of 1.9 Å in the ASQ state compared to 2.5 Å in the OX state confirms a  
25 significantly stronger H-bond to O2 in the <sup>ET</sup>ASQ than in <sup>ET</sup>OX consistent with  
26 stabilization of <sup>ET</sup>ASQ relative to <sup>ET</sup>OX by this interaction, and hence elevation of  
27 <sup>ET</sup>E<sup>o</sup><sub>OX/ASQ</sub>. Thus, we find that the H-bond to <sup>ET</sup>O2 is an important contributor to <sup>ET</sup>flavin's  
28 unusually stable ASQ state.  
29  
30  
31  
32  
33  
34  
35  
36  
37  
38

39 **Figure 6:** Relaxed energy scans along the <sup>ET</sup>O2 H-bond of <sup>ET</sup>flavin for the  $\delta$ H290 systems.  
40 (A) H-bond scanned. (B) Scans of H-bond donated to ET FAD's O2 by  $\delta$ H290. (C) Structure  
41 corresponding to the local energy minimum that appeared at shorter H-bond distances in the  
42 <sup>ET</sup>AHQ $\delta$  state, indicating proton transfer to the <sup>ET</sup>flavin's O2 atom. However, the local energy  
43 minimum was almost 40 kcal/mol higher than the global minimum obtained, corresponding to a  
44 negligible Boltzmann population for this state.  
45  
46  
47  
48  
49

## 50 2.5 The Bf site: H-bonding at <sup>Bf</sup>N5

51 The energy-minimized Bf site structures seemed less responsive to oxidation state  
52 changes than those of the ET site (Table S8, Tables S9 and S10). Additionally, the Bf site  
53 did not donate a H-bond to N1, one of the interactions that may stabilize ASQ in the ET  
54 site (See Scheme 2) [66]. Whereas the ET site displayed a constellation of backbone NHs  
55 donating H-bonds to O4, the energy-minimized Bf site provided only one weak H-  
56  
57  
58  
59  
60  
61  
62  
63  
64  
65

1 mediated interaction ( $\geq 3.4$  Å from A129 amide N to  $^{Bf}O4$ ,  $\geq 2.4$  Å from H to  $^{Bf}O4$ ). Thus,  
2 states and positions with more electron density appear poorly stabilized by H-bonds to  
3 the  $^{Bf}$ flavin, consistent with its less favorable reduction than  $^{ET}$ flavin (Table 1). However,  
4  $^{Bf}OX$  may be better stabilized, as the distance between  $^{Bf}$ flavin's N5 and the H-bond  
5 donating heavy atom was shorter in  $^{Bf}OX$  (2.9 Å) than in the  $^{ET}OX_{\delta}$  and  $^{ET}OX_{\epsilon}$  models  
6 (3.3 and 3.3 Å). This distinction could be a contributor to  $^{Bf}$ flavin's lower  $E^{\circ}$ , so we  
7 investigated further.  
8  
9

10  
11  
12 Relaxed scans of the H-bond between R146 and  $^{Bf}N5$  suggested a weak tendency for  
13  $^{Bf}ASQ$ 's N5 to capture a proton from R146, although that structure was high in energy  
14 and corresponds to the saddle-point at an H-to- $^{Bf}N5$  distance of 1 Å rather than a genuine  
15 local minimum (Figure 7B). We therefore tested the possibility of proton transfer from  
16 R146 to  $^{Bf}N5$  in the other anionic oxidation state, by comparing  $^{Bf}AHQ$  protonated at N5  
17 (the default) with the  $^{Bf}AHQ_{H1}$  tautomer (See Scheme 1). In this case, a defined local  
18 minimum was obtained with a shorter H-to- $^{Bf}N5$  distance that corresponds to proton  
19 transfer from R146 to generate neutral HQ (NHQ, Figure 7B). Given the 12.8 kcal/mol  
20 higher energy of this conformation compared to that of the default  $^{Bf}AHQ$ , it appears that  
21 the NHQ would only be populated to  $3.8 \times 10^{-10}$  (corresponding to a  $pK_a \approx 2.4$ ). However,  
22 it could serve as a transition state in catalysis, for example mediating proton transfer  
23 to/from  $^{Bf}N5$  where the proton would be acquired from NADH.  
24  
25  
26  
27  
28  
29  
30  
31  
32  
33  
34  
35  
36  
37

38 **Figure 7:** Energy profiles of the H-bond donated to  $^{Bf}N5$  as a function of  $^{Bf}$ flavin's oxidation  
39 state. (A) H-bond scanned in the  $^{Bf}$ flavin site. (B) Scans of H-bond between R146 and  $^{Bf}N5$ ,  
40 showing weak inflection points at distances shorter than optimum. The purple curve and  
41 associated points describe  $^{Bf}AHQ$  protonated at N5 whereas the coral pink curve and associated  
42 points describe the  $^{Bf}AHQ_{H1}$  tautomer protonated at N1 instead,  $^{Bf}AHQ_{H1}$ , see Scheme 1 for  
43 structures. The free energy difference between the two minima of  $^{Bf}AHQ_{H1}$  was 4.6 kcal/mol.  
44 The free energy difference between the  $^{Bf}AHQ_{H1}$  minimum and the N5-protonated  $^{Bf}AHQ$   
45 minimum was 8.2 kcal/mol.  
46  
47  
48  
49  
50  
51  
52

### 53 2.6 H-bonding by another rotamer of R146, for the AHQ of $^{Bf}$ flavin

54 Although our energy-minimized  $^{Bf}AHQ$  system was protonated at N5, no potential H-  
55 bond acceptor for H5 was observed following simple geometry optimization starting from  
56 the OX state crystallographic protein geometry. Instead, the H5 of  $^{Bf}AHQ$  was directed  
57 at the side chain of conserved Ile157. This, and the flavin's retention of almost flat  
58  
59  
60  
61  
62  
63  
64  
65

1 geometry in the AHQ state (SI Figure S5), raised concern that our energy minimized  
2  $\text{BfAHQ}$  might not describe the global energy minimum. To test for additional low-energy  
3 conformations of the AHQ Bf site, we surveyed all possible rotamers of R146. Most were  
4 excluded on steric grounds, but two formed favorable H-bonds with  $\text{Bf}$ flavin. After the  
5 standard energy minimization and QM/MM optimization, a conformation was obtained  
6 with a Gibbs free energy only 1 kcal/mol above that of the crystal structure-derived model  
7  $\text{BfAHQ}$  (Table S11). We therefore assessed this structure as an alternative model for the  
8  $\text{BfAHQ}$  state,  $\text{BfAHQ}_{\text{R146}}$ , and henceforth refer to the OX crystal structure-derived models  
9 as  $\text{BfAHQ}_{\text{xtal}}$ . The stability of the alternative conformation seems specific to the AHQ state  
10 as  $\text{OX}_{\text{R146}}$  and  $\text{ASQ}_{\text{R146}}$  models obtained by energy minimization starting from  $\text{BfAHQ}_{\text{R146}}$   
11 with OX or ASQ flavin yielded significantly higher Gibbs free energies compared to the  
12 corresponding  $\text{BfOX}_{\text{xtal}}$  and  $\text{BfASQ}_{\text{xtal}}$  models. Therefore, only  $\text{BfAHQ}_{\text{R146}}$  was pursued.  
13 The finding that this conformation stabilizes specifically the AHQ state makes it an  
14 additional possible contributor to redox tuning.

15  $\text{BfAHQ}_{\text{R146}}$  differed from  $\text{BfAHQ}_{\text{xtal}}$  by reorientation of the R146 side chain to donate a  
16 H-bond to the  $\text{BfO4}$  via the *re* face, as opposed its H-bond donated from the *si* face to  $\text{BfN5}$   
17 in the  $\text{BfOX}_{\text{xtal}}$  structure (Figure 8). A water took the position vacated by R146 and became  
18 a H-bond acceptor from  $\text{BfH5}$ . This greatly improves the site's compatibility with the  
19  $\text{BfAHQ}$ , because N5H is a poor acceptor but a good H-bond donor via H5. Moreover, the  
20 new water near  $\text{BfH5}$  is a much better H-bond acceptor than the side chain of I157. These  
21 can explain why the  $\text{BfAHQ}_{\text{R146}}$  model becomes competitive specifically in the AHQ state.

22 **Figure 8:** Hydrogen bonding with  $\text{Bf}$ flavin in the  $\text{AHQ}_{\text{R146}}$  model. (A) H-bond network in the  
23  $\text{BfAHQ}_{\text{R146}}$  model viewed from *si* face (top) vs. edge-on view of the flavin showing its bent  
24 geometry and H-bonding involving R146 (below). (B) Comparison of the rotamers of R146  
25 present in  $\text{BfAHQ}_{\text{R146}}$  (green flavin) and  $\text{BfAHQ}_{\text{xtal}}$  models (purple flavin, as in Figure 7).

26 Reorientation of R146's side chain also resulted in a new H-bond from it to  $\text{BfO4}$   
27 (Figure 8). This joined the H-mediated interaction from the backbone NH of A129 (Figure  
28 8A). However, the new H-bond from R146's side chain was stronger than that from A129,  
29 based on a distance of 2.7 Å between R146's  $\text{N}\eta_1$  and  $\text{BfO4}$  (vs. 3.0 Å from A129-N to  
30  $\text{BfO4}$ , Table S12 and Figure S6), consistent with R146's positive charge and more labile  
31  $\text{H}\eta_1$  vs. the backbone amide NH of A129. This new stronger H-bond can explain the

1 greater negative charge that accumulated at  $^{Bf}O4$  upon formation of flavin  $^{Bf}AHQ_{R146}$ ,  
2 compared to  $^{Bf}AHQ_{xtal}$  (Figure S8). In turn, the greater charge density at  $^{Bf}O4$  makes sense  
3 of A129's H-bond to  $^{Bf}O4$  being shorter (stronger) in  $^{Bf}AHQ_{R146}$  where it shares  $^{Bf}O4$  with  
4 R146, than in  $^{Bf}AHQ_{xtal}$ . The pattern included H-bond contractions at  $^{Bf}O2$  and  $^{Bf}N3H$  as  
5 well, albeit smaller. Thus, R146's reorientation and recruitment of a better H-bond  
6 acceptor for  $^{Bf}N5H$  appear to produce a generally more favorable complex in  $^{Bf}AHQ_{R146}$ ,  
7 based on geometrical and electrostatic criteria.

8  
9  
10  
11  
12 Finally, the  $^{Bf}AHQ_{R146}$  model escaped the perplexing OX-like geometry retained by  
13 the  $^{Bf}AHQ_{xtal}$  model.  $^{Bf}AHQ_{R146}$  deviated considerably from planarity (Figures 8A and  
14 9C), in agreement with structural studies of numerous other reduced flavin sites  
15 [28,29,72]. Thus the  $^{Bf}AHQ_{R146}$  model provides a chemically and energetically plausible  
16 additional conformation to describe the AHQ state of the Bf site.  
17  
18  
19  
20  
21  
22  
23  
24  
25  
26

27 **Figure 9:** Analysis of steric and electrostatic effects of protein environment on  $^{Bf}FAD$   
28 comparing the crystal structure-derived model  $^{Bf}AHQ_{xtal}$  with the  $^{Bf}AHQ_{R146}$ . (A) Isoalloxazine  
29 color coded by charge difference between protein electrostatic environment and frozen gas  
30 phase. (B) Dihedral angles used to quantify the butterfly bending. (C) Bar plots of the dihedral  
31 angles comparing the butterfly bending of the of  $^{Bf}AHQ_{xtal}$  with  $^{Bf}AHQ_{R146}$ .  
32  
33  
34  
35  
36

### 37 3. Discussion

38  
39 Beginning with the crystal structure of OX *Afe*ETF, we examined the effect of placing  
40 the flavin in each of the three oxidation states known for this system, for each of the two  
41 flavins. To generate optimized sites, we used MM energy minimization followed by  
42 QM/MM geometry optimization treating the flavin quantum mechanically and relaxing  
43 residues with any atom within 5 Å. Despite its simplicity, this protocol documented  
44 reorientation of a side chain, 1 Å repositioning of a loop of backbone and reorganization  
45 of a critical H-bonding network supporting the redox-active N5 [37], for the ET site. The  
46 Bf site did not adapt in the course of energy minimization when different oxidation states  
47 of the flavin were embedded in it. However, a screen of alternative rotamers for side  
48 chains able to H-bond with the  $^{Bf}$ flavin revealed an additional energetically-viable  
49 conformation. For both sites, H-bonds of interest were characterized via constrained  
50 variation of the lengths of H-bonds donated to N5, in each flavin oxidation state, with the  
51  
52  
53  
54  
55  
56  
57  
58  
59  
60  
61  
62  
63  
64  
65

1 H-bond donor included in the quantum regime. This protocol yielded profiles of energy  
2 vs. H-bond length that identify H-bonds related to redox tuning. Our studies revealed  
3 three overarching distinctions between the two flavin sites that suggest explanations for  
4 their contrasting reactivities.  
5  
6

### 7 3.1 Adaptive network of H-mediated interactions surrounding N5 in the ET site

8  
9 Whereas the ET site has a highly adaptive network of multiple weak interactions  
10 supporting  ${}^{\text{ET}}\text{N5}$  and accommodating its acquisition of  ${}^{\text{ET}}\text{H5}$ , the Bf site resisted redox-  
11 coupled change. This may suppress the  ${}^{\text{Bf}}\text{ASQ}$  state in so far as reduction by only one  
12 equivalent may not suffice to drive any conformational change needed to stabilize  
13 reduced  ${}^{\text{Bf}}$ flavin. Full reduction and protonation of  ${}^{\text{Bf}}$ flavin may be required to elicit  
14 conformational accommodation by this site, where several important H-bonds derive  
15 from backbone (T94'- ${}^{\text{Bf}}\text{O2}$ , L127'- ${}^{\text{Bf}}\text{N3H}$ , A129'- ${}^{\text{Bf}}\text{O4}$ ).  
16  
17  
18  
19  
20  
21

22 As part of the ET site's adaptive response, the side chain of Q266 reoriented during  
23 energy minimization in  ${}^{\text{ET}}\text{AHQ}$ . This reversed orientation of the corresponding Gln was  
24 recently reported in the crystal structure of lactate dehydrogenase's confurcating ETF  
25 (7QH2.pdb [16]), although we caution that the protein database contains several instances  
26 of Gln and Asn side chains whose orientations appear to have escaped scrutiny. H-  
27 mediated interactions at  ${}^{\text{ET}}\text{N5}$  were weak based on their lengths, but the conformation  
28 with the shorter S270 -  ${}^{\text{ET}}\text{N5}$  distance attained greater significance relative to the second  
29 energy minimum, becoming better defined, in the  ${}^{\text{ET}}\text{ASQ}$  state. This is consistent with  
30 observed depression of the  $E^{\circ}_{\text{OX/ASQ}}$  of  ${}^{\text{ET}}$ flavin upon replacement of the residue  
31 analogous to S270 [37].  
32  
33  
34  
35  
36  
37  
38  
39

40 In contrast, geometry optimization of Bf site models did not cause significant  
41 displacements. We propose that this reflects considerably steeper energy barriers to  
42 reorganization in the Bf site, rather than absence of other local energy minima, since a  
43 plausible alternative conformation was identified. An expanded approach including  
44 heating and annealing, and/or full molecular dynamics, is needed to sample the  
45 conformational space.  
46  
47  
48  
49  
50

51 Indeed, we have shown that  ${}^{\text{Bf}}$ flavin's AHQ state can favorably engage R146 in a  
52 conformation different from that seen in  ${}^{\text{Bf}}\text{AHQ}_{\text{xtal}}$ . Migration of R146 from donating a  
53 H-bond to N5 in  ${}^{\text{Bf}}\text{OX}$  and  ${}^{\text{Bf}}\text{ASQ}$ , to donating to  ${}^{\text{Bf}}\text{O4}$  of  ${}^{\text{Bf}}\text{AHQ}$ , is consistent with the  
54 chemical nature of Arg's side chain, which constrains it to always donate a H-bond. In  
55 contrast, the N5 of flavin changes from being a H-bond acceptor in the OX and ASQ  
56  
57  
58  
59  
60  
61  
62  
63  
64  
65



1 states to a donor in AHQ, prompting reorganization of H-bonding partners. For <sup>ET</sup>flavin  
2 this was accomplished by S270 changing allegiance from being a donor to <sup>ET</sup>N5, to  
3 donating to Y37' instead, while *accepting* a H-bond donated by <sup>ET</sup>H5. In the Bf site, the  
4 <sup>Bf</sup>AHQ<sub>R146</sub> model allows R146 to continue to stabilize the anionic <sup>Bf</sup>flavin's net charge  
5 via H-bond donation to <sup>Bf</sup>O4, even when <sup>Bf</sup>N5 is protonated. We speculate that an  
6 alternative rotamer of R146 may also explain <sup>Bf</sup>ASQ stabilization in response to  
7 perturbations such as depletion of <sup>ET</sup>FAD [73]. Furthermore, if R146's conformation is  
8 responsive to events in the shuttle domain where <sup>ET</sup>flavin resides, then the reverse would  
9 also be true, and adoption of the <sup>Bf</sup>AHQ<sub>R146</sub> rotamer could contribute to a conformational  
10 response on the part of the shuttle domain. Indeed, R146 is modelled in a variety of  
11 distinct rotamers among crystal structures of Bf-ETFs (SI Figure S7).  
12  
13  
14  
15  
16  
17  
18  
19

### 20 3.2 Coupling to domain-scale conformation?

21 The fact that multiple configurations of H-bonding with <sup>ET</sup>N5 have comparable  
22 energies appears to reflect an underlying network of H-bonds including the side chain of  
23 Y37' as well as the S270 we investigated (Figure S4). Interestingly, Y37' resides in the  
24 other subunit of *Afe*ETF, in the base domain, whereas <sup>ET</sup>flavin is bound in the shuttle  
25 domain (Figures 1, S1). Only the closed conformation of *Afe*ETF shown in Figure 1  
26 permits H-bonding between S270 and Y37' as they are separated by more than 20 Å in  
27 the open conformation (Figure S1 [14,15]). Thus, the Y37' - S270 - <sup>ET</sup>N5 network could  
28 modulate the relative energies of the two conformations of *Afe*ETF in response to  
29 <sup>ET</sup>flavin's oxidation state. The domain scale alternation of conformations is observed even  
30 for canonical ETFs that lack a <sup>Bf</sup>flavin, consistent with triggering events emanating from  
31 the ET site. We also note that depletion of the <sup>ET</sup>flavin leads to a change in the redox  
32 reactivity of the <sup>Bf</sup>flavin [73], confirming mutational evidence that events in one site can  
33 affect the other [34]. The current local energy minimizations cannot address such long-  
34 range effects, but can identify local changes that could trigger them. Thus, the  
35 reorientation of Q266 upon reduction of <sup>ET</sup>flavin is noteworthy. Importantly, the 1 Å shift  
36 seen in G271's backbone upon <sup>ET</sup>flavin reduction may also be significant to the  
37 conformational change, because G271 resides in a loop that forms part of the shuttle  
38 domain's interface with the base.  
39  
40  
41  
42  
43  
44  
45  
46  
47  
48  
49  
50  
51  
52  
53

### 54 3.3 H-bond from His to <sup>ET</sup>flavin O2 may stabilize ASQ and support 1e reactivity

55 We demonstrated that a conserved His in the ET site donates a H-bond to the flavin  
56 <sup>ET</sup>O2 and stabilizes excess negative charge there, especially in the <sup>ET</sup>ASQ state. We tested  
57  
58  
59  
60  
61  
62  
63  
64  
65

1 the significance of this H-bond, via comparison of models containing the  $\delta$ -tautomer of  
2 H290 which forms the H-bond, vs. models containing the  $\epsilon$ -H290 and retaining all the  
3 same atoms but no H-bond between H290 and  $^{ET}O_2$ . Such targeted tests are rarely  
4 possible in experiments, highlighting the value of computations (but see [74]). The  
5 significance of this H-bond is nevertheless supported by the experiments of evolution, as  
6 H290 is 90% conserved and so is the Y279 that supports it. Crucially, Y279 is expected  
7 to be protonated at neutral pH, and therefore to be a H-bond donor to H290. This in turn  
8 will polarize H290, defining it as an acceptor from Y279 and therefore a donor to  $^{ET}O_2$ .  
9

10 Because  $^{ET}O_2$  is *para* to  $^{ET}N_5$ , it has considerable inductive influence over the redox-  
11 active  $^{ET}N_5(H)$ . In  $\delta$ -His290 systems, the shorter and longer interactions between S270  
12 and  $^{ET}N_5$  were comparably favorable in  $^{ET}OX$  and  $^{ET}AHQ$  (Figure 5C). This is consistent  
13 with a shift of excess negative charge to  $^{ET}O_2$  from  $^{ET}N_5$ , making the shorter-distance  
14 energy well at  $^{ET}N_5$  less deep. The potency of  $O_2$ 's remote effect on  $N_5$  reflects the  $OX$   
15 state's highly correlated electronic structure [75].  
16

17 A comparable interaction was not seen in the Bf site, where  $^{Bf}O_2$  H-bonds with a  
18 molecule of water in the crystal structure of *AfeETF*. Water is more likely to adapt to  
19 demands made by the flavin than to impose constraints upon it, since water can reorient  
20 and reposition to minimize strain. Nevertheless, that water molecule appears to H-bond  
21 to the side chain of D93' which is 100% conserved (in a set of 228 group II Bf-ETF non-  
22 basal sequences [38]). This will make the water a poor H-bond donor to  $^{Bf}O_2$ ,  
23 rationalizing the deficit of electron density on  $^{Bf}$ flavin's  $^{Bf}O_2$  revealed by our NBO  
24 calculations in all three oxidation states (Figure 3). We propose that poor H-bond  
25 donation to  $^{Bf}O_2$  contributes to the Bf site's suppression of  $^{Bf}ASQ$ . Additionally, although  
26 R146 donates a H-bond to  $^{Bf}N_5$  that might be thought to stabilize  $^{Bf}ASQ$  on electrostatic  
27 grounds, it concentrates excess electron density on  $^{Bf}N_5$  (Figure 4) creating a deficit at  
28  $^{Bf}O_2$  that is not favorable, given the strong electronegativity of the  $N_1-O_2$  locus.  
29

30 In the AHQ oxidation state, the  $^{Bf}AHQ_{R146}$  model results in a very different distribution  
31 of excess electron density from that stabilized in  $^{Bf}AHQ_{xtal}$ , with the H-bond from R146  
32 drawing electron density to  $^{Bf}O_4_{R146}$  (Figure 9A), rather than  $^{Bf}N_5$  as in  $^{Bf}AHQ_{xtal}$  (Figure  
33 3). The smaller electron density deficit on  $O_2$  in  $^{Bf}O_2_{R416}$  may be because  $O_4$  is in the  
34 *meta*-position relative to  $O_2$ , whereas  $N_5$  is in *para*.  
35

36 Thus, we have identified H-bonding that can explain an unfavorable electron density  
37 deficit at  $O_2$  that is particularly acute in the  $^{Bf}ASQ$  (Figure 3), whereas altered H-bonding  
38 in  $^{Bf}AHQ_{R146}$  enables the site to stabilize the same net charge in the AHQ. Together with  
39  
40  
41  
42  
43  
44  
45  
46  
47  
48  
49  
50  
51  
52  
53  
54  
55  
56  
57  
58  
59  
60  
61  
62  
63  
64  
65

1 the native reactivity of flavins, these two features can rationalize the Bf site's suppression  
2 of ASQ and 1e reactivity, in favor of the 2e reactivity that characterizes bifurcating sites.  
3 This is in striking contrast with the ET site, where 1e reactivity results from stabilization  
4 of ASQ we could attribute substantially to H-bonding to O2.  
5  
6  
7

#### 8 **4. Concluding Remarks**

9  
10 We employed computations to learn about reduced states not captured yet in crystal  
11 structures, including states such as the postulated high-energy ASQ state of Bf flavin  
12 which is not normally stable enough to permit spectroscopic study. Our calculations  
13 assuming the closed conformation reproduce the observed contrasting reactivities of the  
14 two flavins. Thus, they succeed in modeling the protein features that stabilize the ASQ  
15 state in the ET site but not the Bf site, as well as features that disfavor reduction of the Bf  
16 flavin more than the ET flavin. Our calculations show that the extraordinary stability of  
17 <sup>ET</sup>flavin's ASQ state can be attributed substantially to a single H-bond, from H290 to  
18 <sup>ET</sup>ASQ's O2. Formation of the AHQ state of ET flavin, including acquisition of a proton  
19 at N5, was associated with a change in the preferred orientation of Q266, displacement  
20 of a backbone loop and reorganization of an interaction network spanning domains and  
21 subunits. Additionally, we raise the possibility that the side chain of R146 reorients upon  
22 reduction of the Bf flavin, and forms different H-bonds. New H-bond donation to the Bf  
23 flavin's O4 is consistent with this flavin's lower  $E^{\circ}_{OX/AHQ}$  while the absence of a good H-  
24 bond donor to N1 and O2 can explain this flavin's suppressed ASQ that contrasts with  
25 that of the ET flavin.  
26  
27  
28  
29  
30  
31  
32  
33  
34  
35  
36  
37  
38  
39  
40

#### 41 **5. Experimental Procedures**

##### 42 5.1 General approach

43  
44 The starting coordinates for the Bf-ETF of *Acidaminococcus fermentans* (*Afe*ETF)  
45 were retrieved from the crystal structure (4KPU.pdb [39]). Apart from the  
46 crystallographic waters present in the crystal structure, additional water molecules were  
47 added with Dowser++ [40] (3 water molecules within 5 Å of <sup>Bf</sup>FAD and 7 water  
48 molecules within 5 Å of <sup>ET</sup>FAD), resulting in a total 607 water molecules. A total of 11  
49 systems were defined (Table 2), where the oxidation state and selected additional  
50 properties of the flavin of interest were varied. The model <sup>Bf</sup>AHQ<sub>R146</sub> will be discussed at  
51 the end of this section.  
52  
53  
54  
55  
56  
57  
58  
59  
60  
61  
62  
63  
64  
65

1  
2 >>Table 2 belongs here<<  
3  
4  
5

### 6 5.1.1 Relaxation via molecular mechanical (MM) energy minimization

7 MM energy minimization was performed with the 'pmemd' software from AMBER18  
8 [41] on each of the systems in Table 2. Structures were preprocessed with 'tleap' to obtain  
9 topology and coordinate files for AMBER [41]. The ff19SB force field was defined for  
10 protein residues [42], while the GAFF force field was implemented for FAD [43,44].  
11 Parameters for FAD in the canonical oxidation states were calculated with RESP [45] and  
12 Antechamber [43,44,46]. Parameters are listed in SI. Only the <sup>Bf</sup>AHQ<sub>H1</sub> system could not  
13 be relaxed via MM energy minimization, as no parameters were calculated.  
14  
15

16 The 607 water molecules were defined as TIP3P waters. The total charge of each  
17 system was neutralized with addition of Na<sup>+</sup> ions (19 ions in OX systems, and 20 ions in  
18 ASQ and AHQ systems), which were allowed to adopt energy minimizing locations. The  
19 MM energy minimization was performed in two steps, 5·10<sup>3</sup> cycles of steepest descent  
20 followed by 5·10<sup>3</sup> cycles using the conjugate gradient method. A restraining force of 100  
21 kcal·mol<sup>-1</sup>·Å<sup>-2</sup> was applied on solute atoms during the energy minimization to prioritize  
22 relaxation of solvent. The electrostatic cut-off value was 10 Å and the effective Born  
23 radius was set to 25 Å in lieu of a water box.  
24  
25

26 The relaxed computational models were assessed using MolProbity, which scores for  
27 avoidance of unfavorable Ramachandran angles, van der Waals clashes and improbable  
28 rotamers [47]. All the structures of this study displayed MolProbity scores better than that  
29 of the parent crystal structure and were in the 100<sup>th</sup> percentile (Table S13). The RMSD  
30 vs. the crystal structure (4KPU.pdb) was always below 0.85 Å (Table S14).  
31  
32

### 33 5.1.2 Hybrid quantum mechanical / molecular mechanical geometry optimization

34 Geometries were optimized via quantum mechanical / molecular mechanical  
35 (QM/MM) energy minimization using B3LYP/cc-pVDZ with D3BJ dispersion correction  
36 using the structures obtained from initial MM energy minimization. As no MM energy  
37 minimization was performed for the <sup>Bf</sup>AHQ<sub>H1</sub> model, relaxed coordinates from the  
38 <sup>Bf</sup>AHQ model were adopted, the H5 atom was removed and a H was placed near N1. The  
39 QM region consisted of the lumiflavin moiety of the flavin of interest (Scheme 1, 30  
40 atoms in OX and ASQ systems, and 31 atoms in AHQ systems). The MM region was  
41 defined as the rest of the atoms, where the two following groups of atoms were allowed  
42  
43  
44  
45  
46  
47  
48  
49  
50  
51  
52  
53  
54  
55  
56  
57  
58  
59  
60  
61  
62  
63  
64  
65

1  
2  
3  
4  
5  
6  
7  
8  
9  
10  
11  
12  
13  
14  
15  
16  
17  
18  
19  
20  
21  
22  
23  
24  
25  
26  
27  
28  
29  
30  
31  
32  
33  
34  
35  
36  
37  
38  
39  
40  
41  
42  
43  
44  
45  
46  
47  
48  
49  
50  
51  
52  
53  
54  
55  
56  
57  
58  
59  
60  
61  
62  
63  
64  
65

to move: side chains including an atom within 5 Å of the FAD of interest, and backbone atoms forming H-bonds with the isoalloxazine ring system of interest. The same AMBER force field parameters were employed as for energy minimization, with exception that the cut-off value for non-bonded interactions was defined as 30 Å. Chemshell version 3.7 was employed to interface ORCA 4.2.1 with AMBER 18 [41,48] and to treat the boundary with electrostatic embedding and a hydrogen link scheme [49,50]. QM/MM geometry optimizations were performed using the ‘DL-FIND’ module [51].

H-bonds are understood to combine some covalent character with a predominantly electrostatic (Coulomb) attraction. The covalent component includes steric constraints to produce orientational preferences for shorter H-bonds [52,53], while the electrostatic component extends over longer distances [54-56]. Although distance between donor and acceptor is not an ideal criterion for determining whether or not a H-bond is present [57], it is well understood and readily measured. A comparison of heavy atom to heavy atom distances deemed to encompass the majority of H-bonds in proteins yields a value of 3.2 Å for the types of H-bonds we studied [58,59], which mostly involve an NH group as the H-bond donor and an O as the recipient. OH donors are recognized to produce slightly shorter H-bonds while N atom acceptors produce slightly longer ones [54,58,59]; however considering that our uncertainties are on the order of these 0.1 Å differences, we retained a common threshold of 3.2 Å for the sake of simplicity. Additionally, the distance between the acceptor heavy atom and the H atom mediating the interaction is 2.1 Å or shorter in 80-90% of H-bonds in a survey of high-resolution crystal structures [54]. To provide an inclusive picture, instances satisfying either of these conditions were deemed to represent H-bonds. Interactions over longer distances and a wide range of geometries have been noted in networks of multiple H-bonds [60], especially in connection with aliphatic hydroxyl groups [54]. We interpreted these as weaker interactions that are expected to lack orientational preference due to negligible covalent character [54]. Therefore, they are described as 'H-mediated interactions' [59]. Throughout, 'donation' or 'acceptance' of a H-bond is discussed in terms of donation/acceptance of the H.

### 5.1.3 Free energy changes associated with reduction and proton acquisition

Free energy changes between flavin oxidation states were calculated to assess energies associated with reduction and proton acquisition. These values do not correspond to  $E^\circ$ s because the two states being compared have different numbers of electrons (and protons). However, the energies associated with a given change can be compared for the two flavin

1 sites, to learn which site best stabilizes reduction or proton acquisition, and to ask how  
2 the effect is produced by the protein environment. Gibbs free energy values were  
3 calculated using QM/MM and the same level of theory as for the geometry optimizations.  
4

5 As reference, the corresponding free energy changes were calculated for isolated  
6 lumiflavin. DFT geometry optimizations were performed for lumiflavin in the OX, ASQ  
7 and AHQ states in gas phase with B3LYP/cc-pVDZ and D3BJ dispersion correction.  
8  
9  
10  
11  
12  
13  
14  
15  
16  
17  
18  
19  
20  
21  
22  
23  
24  
25  
26  
27  
28  
29  
30  
31  
32  
33  
34  
35  
36  
37  
38  
39  
40  
41  
42  
43  
44  
45  
46  
47  
48  
49  
50  
51  
52  
53  
54  
55  
56  
57  
58  
59  
60  
61  
62  
63  
64  
65

Gibb's free energy values were calculated using DFT using the same level of theory as for the geometry optimizations.

#### 5.1.4 Calculation of Natural Bond Order electron densities (NBOs) in presence and absence of protein environment

Calculations of NBOs of flavin models were performed in presence and absence of the protein environment using the optimized QM/MM geometries. In the latter case, points charges in the protein were omitted but the optimized QM/MM flavin geometry was retained. Therefore, calculations in absence of the protein environment were called "frozen gas-phase" NBO. The same level of theory was implemented as for QM/MM and energy calculation.

#### 5.1.5 Relaxed energy scans along N5 and O2 H-bonds

The QM region was enlarged for the following QM/MM calculations to include the side chain atoms of the amino acid participating in the H-bond of interest (18 more atoms for R146, 5 atoms for S270, and 11 atoms for H290). Geometries were reoptimized applying the enlarged QM regions with B3LYP/cc-pVDZ and dispersion correction as in previous sections. Subsequently, two constraints were implemented, similarly to Tsujimura and Ishikita [61]: the distance between the participating proton and the H-bond acceptor, and the distance between the two heavy atoms of the H-bond. These distances were constrained with a harmonic constant of 6 Hartree/Bohr<sup>2</sup>. The reference distance between the H-bond acceptor and the proton was varied in 0.1 Å steps whereas the reference distance between heavy atoms was set to the previously optimized QM/MM values. In performing relaxed energy scans, the relaxed geometry with the most similar constraint value was used as input for the next constrained geometry optimization.

For each proton position, the Gibbs free energy was calculated using QM/MM and the same level of theory as for the geometry optimizations. These values are plotted vs. proton - H-bond acceptor distance in the figures. Difficulties were encountered in the Gibbs free energy calculation for the energy-relaxed scans of the N5 H-bond of the <sup>ET</sup>ASQ<sub>6</sub> and

<sup>ET</sup>ASQ<sub>δ</sub> models. For these energy scans, only electronic energies are reported here. We attribute the difficulties to the large distance between the flavin and the S270 side chain.

Local energy minima were validated via frequency analysis with DFT using B3LYP/cc-pDVZ and D3BJ dispersion correction. Coordinates of the lumiflavin moiety of the studied flavin and those of all residues in the first coordination sphere were included (266 atoms in <sup>Bf</sup>OX and <sup>Bf</sup>ASQ; 270 atoms in <sup>Bf</sup>AHQ and <sup>Bf</sup>AHQ<sub>H1</sub>; 257 atoms in <sup>ET</sup>OX<sub>ε</sub>; 254 atoms in <sup>ET</sup>OX<sub>δ</sub>; 248 atoms in <sup>ET</sup>ASQ<sub>ε</sub>; 251 atoms in <sup>ET</sup>ASQ<sub>δ</sub>; 252 atoms in <sup>ET</sup>AHQ<sub>ε</sub>; and 249 in <sup>ET</sup>AHQ<sub>δ</sub> models).

## 5.2 Additional models.

For <sup>Bf</sup>flavin, additional models were considered. Working with the coordinates of the OX crystal structure 4KPU.pdb [39], we screened all the rotamers of R146 in Chimera's library [62,63], reorienting the nearby side chain of C128 when warranted. Most rotamers were excluded on the basis of steric clashes. The two that minimized clashes and formed a H-bond with the flavin were refined by MM energy minimization followed by hybrid QM/MM geometry optimization with the AHQ state of the <sup>Bf</sup>flavin, implementing the standard protocol (above). One of the resulting structures had an energy only 1 kcal/mol higher than that of the <sup>Bf</sup>AHQ obtained from the crystal structure, and was considered further as <sup>Bf</sup>AHQ<sub>R146</sub> (Table 2).

We also screened alternative rotamers of the other amino acid side chain capable of H-bonding with the <sup>Bf</sup>flavin: T94'. After energy minimization, none H-bonded with the flavin. Indeed, the corresponding residue is Val in a lactate dehydrogenase-associated Bf-ETF [16], demonstrating that H-bonding from the side chain is not mandatory.

## Data Availability

Data are provided either within the manuscript or as part of the supporting information.

## Supporting information

This article is accompanied by supporting information [14-16,19,39].

## Acknowledgements

AFM acknowledges partial support from N.S.F. CHE 2108134, D.O.E. DE-SC0021283, KY-EPSCoR PON2 635 2000003148, WDW for vital assistance and RNM for perseverance. We thank the Einstein Foundation of Berlin for funding to RKK, a

1  
2  
3  
4  
5  
6  
7  
8  
9  
10  
11  
12  
13  
14  
15  
16  
17  
18  
19  
20  
21  
22  
23  
24  
25  
26  
27  
28  
29  
30  
31  
32  
33  
34  
35  
36  
37  
38  
39  
40  
41  
42  
43  
44  
45  
46  
47  
48  
49  
50  
51  
52  
53  
54  
55  
56  
57  
58  
59  
60  
61  
62  
63  
64  
65

visiting fellowship to AFM, and ongoing support to MGV via the Einstein Center for Catalysis. MAM's research was funded by the Deutsche Forschungsgemeinschaft (DFG, German Research Foundation) under SFB1078, project C2. RKK thanks DST-SERB for a start-up grant (SRG/2022/000858).

## 6. References

1. Beinert, H. (1956) Spectral characteristics of flavins at the semiquinoid oxidation level. *J. Am. Chem. Soc.* **78**, 5323-5328
2. Thorpe, C. (1991) Electron-Transferring Flavoproteins. in *Chemistry and Biochemistry of Flavoenzymes* (Müller, F. ed.), CRC press, Boca Raton FL. pp 471-486
3. Watmough, N. J., Kiss, J., and Frerman, F. E. (1992) Structural and redox relationships between *Paracoccus denitrificans*, porcine and human electron-transferring flavoproteins. *Eur. J. Biochem.* **205**, 1089-1097
4. Toogood, H. S., van Thiel, A., Scrutton, N. S., and Leys, D. (2005) Stabilization of non-productive conformations underpins rapid electron transfer to electron transferring flavoprotein. *J. Biol. Chem.* **280**, 30361-30366
5. Whitfield, C. D., and Mayhew, S. G. (1974) Purification and properties of electron-transferring flavoprotein from *Peptostreptococcus elsdenii*. *J Biol Chem* **249**, 2801-2810
6. Mohamed-Raseek, N., Duan, H. D., Mroginski, M. A., and Miller, A. F. (2019) Spectroscopic, thermodynamic and computational evidence of the locations of the FADs in the nitrogen fixation-associated electron transfer flavoprotein. *Chem. Sci.* **10**, 7762-7772
7. DuPlessis, E. R., Rohlf, R. J., Hille, R., and Thorpe, C. (1994) Electron-transferring flavoproteins from pig and the methylotrophic bacterium W3A1 contains AMP as well as FAD. *Biochem. Mol. Biol. Int.* **32**, 195-199
8. Sato, K., Nishina, Y., and Shiga, K. (1993) Electron-transferring flavoprotein has an AMP-binding site in addition to the FAD-binding site. *J Biochem* **114**, 215-222
9. Nitschke, W., and Russell, M. J. (2012) Redox bifurcations: Mechanisms and importance to life now, and at its origin. *Bioessays* **34**, 106-109
10. Buckel, W., and Thauer, R. K. (2018) Flavin-based electron bifurcation, a new mechanism of biological energy coupling. *Chem. Rev.* **118**
11. Peters, J. W., Miller, A. F., Jones, A. K., King, P. W., and Adams, M. W. (2016) Electron bifurcation. *Curr. Opin. Chem. Biol.* **31**, 146-152
12. Buckel, W., and Thauer, R. K. (2013) Energy conservation via electron bifurcating ferredoxin reduction and proton/Na<sup>+</sup> translocating ferredoxin oxidation. *Biochim. Biophys. Acta.* **1827**, 94-113
13. Herrmann, G., Jayamani, E., Mai, G., and Buckel, W. (2008) Energy conservation via electron-transferring flavoprotein in anaerobic bacteria. *J. Bacteriol.* **190**, 784-791
14. Demmer, J. K., Bertsch, J., Oppinger, C., Wohlers, H., Kayastha, K., Demmer, U., Ermler, U., and Müller, V. (2018) Molecular basis of the flavin-based electron-bifurcating caffeyl-CoA reductase reaction. *FEBS Lett.* **592**, 332-342
15. Demmer, J. K., Chowdhury, N. P., Selmer, T., Ermler, U., and Buckel, W. (2017) The semiquinone swing in the bifurcating electron transferring flavoprotein/butyryl-coA dehydrogenase complex from *Clostridium difficile*. *Nat. Commun.* **8**, 1577
16. Kayastha, K., Katsyv, A., Himmrich, C., Welsch, S., Schuller, J. M., Ermler, U., and Müller, V. (2022) Structure-based electron-confurcation mechanism of the Ldh-EtfAB complex. *eLife* **11**, e77095
17. Duan, H. D., Mohamed-Raseek, N., and Miller, A. F. (2020) Spectroscopic evidence for direct flavin-flavin contact in a bifurcating electron transfer flavoprotein. *J. Biol. Chem.* **295**, 12618-12634

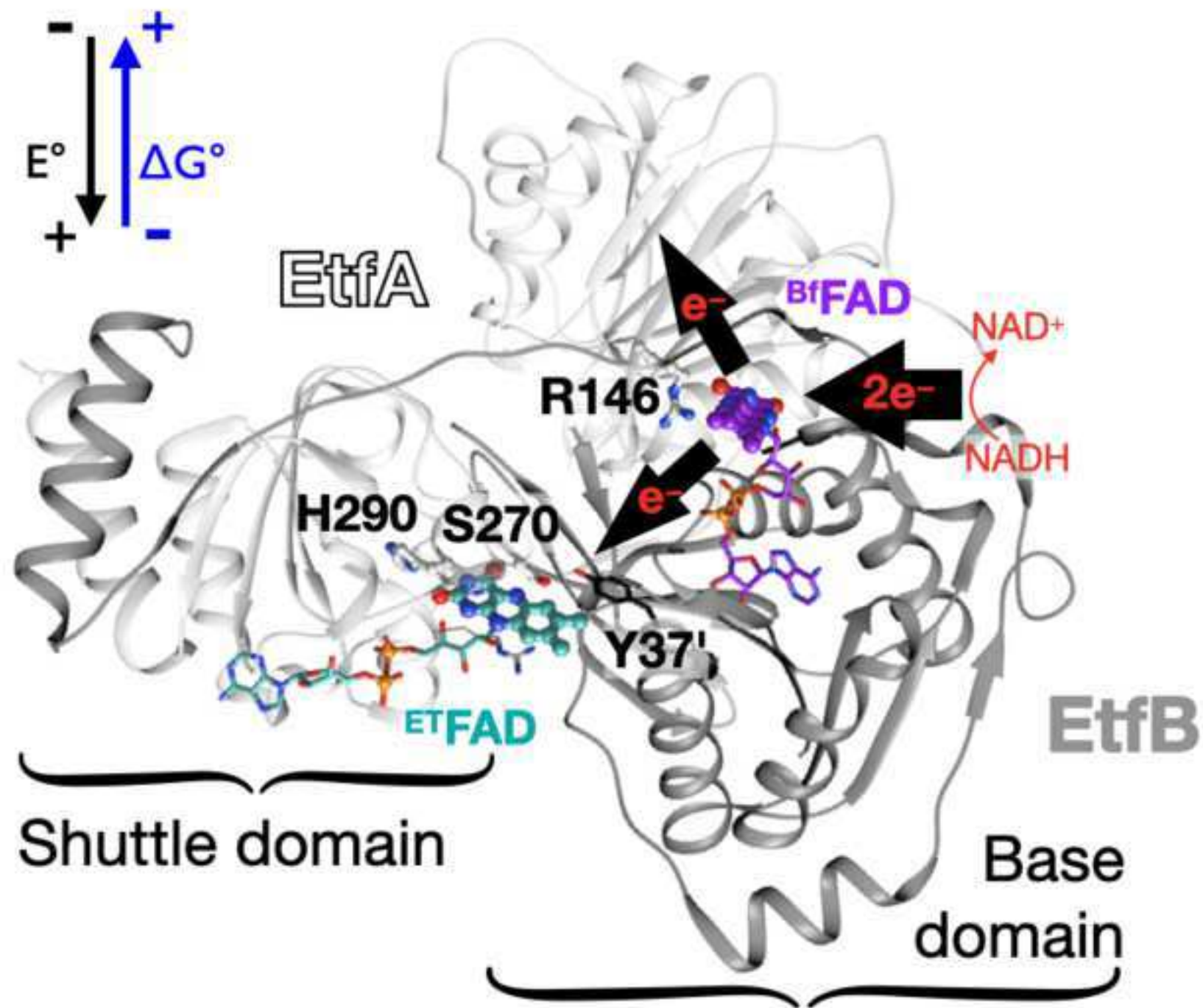


18. Leys, D., Basran, J., Talfournier, F., Sutcliffe, M. J., and Scrutton, N. S. (2003) Extensive conformational sampling in a ternary electron transfer complex. *Nat. Struct. Biol.* **10**, 219-225
19. Feng, X., Schut, G. J., Lipscomb, G., Li, H. Y., and Adams, M. W. W. (2021) Cryoelectron microscopy structure and mechanism of the membrane-associated electron-bifurcating flavoprotein Fix/EtfABCX. *Proc. Natl. Acad. Sci. U. S. A.* **118**, e2016978118
20. Duan, H. D., Lubner, C. E., Tokmina-Lukaszewska, M., Gauss, G. H., Bothner, B., King, P. W., Peters, J. W., and Miller, A. F. (2018) Distinct flavin properties underlie flavin-based electron bifurcation within a novel electron-transferring flavoprotein FixAB from *Rhodopseudomonas palustris*. *J. Biol. Chem.* **293**, 4688-4701
21. Schut, G. J., Mohamed-Raseek, N. R., Tokmina-Lukaszewska, M., Mulder, D. E., Nguyen, D. M. N., Lipscomb, G. L., Hoben, J. P., Patterson, A., Lubner, C. E., King, P. W., Peters, J. W., Bothner, B., Miller, A. F., and Adams, M. W. W. (2019) The catalytic mechanism of electron bifurcating electron transfer flavoproteins (ETFs) involves an intermediary complex with NAD<sup>+</sup>. *J. Biol. Chem.* **294**, 3271-3283
22. Massey, V., and Hemmerich, P. (1980) Active site probes of flavoproteins. *Biochem. Soc. Trans.* **8**, 246-257
23. Fagan, R. L., and Palfey, B. A. (2010) Flavin-dependent enzymes. in *Comprehensive Natural Products Chemistry II* (Begley, T. ed.), Elsevier, Oxford, UK. pp 37-114
24. Mayhew, S. G. (1999) The Effects of pH and Semiquinone Formation on the Oxidation-Reduction Potentials of Flavin Mononucleotide: A Reappraisal. *Eur. J. Biochem.* **265**, 698-702
25. Land, E. J., and Swallow, A., J. (1966) One-electron reactions in biochemical systems as studied by pulse radiolysis. II. Riboflavine. *Biochem* **5**, 2117-2125
26. Roberts, D. L., Salazar, D., Fulmer, J. P., Frerman, F. E., and Kim, J. J. (1999) Crystal structure of *Paracoccus denitrificans* electron transfer flavoprotein: structural and electrostatic analysis of a conserved flavin binding domain. *Biochemistry* **38**, 1977-1989
27. Iijima, M., Ohnuki, J., Sato, T., Sugishima, M., and Takano, M. (2019) Coupling of redox and structural states in cytochrome P450 reductase studied by molecular dynamics simulation. *Scientific reports* **9**, 9341
28. Walsh, J. D., and Miller, A.-F. (2003) Flavin reduction potential tuning by substitution and bending. *J. Mol. Struct. (Theochem)* **623**, 185-195
29. Hasford, J. J., Kemnitzer, W., and Rizzo, C. J. (1997) Conformational effects on flavin redox chemistry. *J. Org. Chem.* **62**, 5244-5245
30. Hazekawa, I., Nishina, Y., Sato, K., Shichiri, M., Miura, R., and Shiga, K. (1997) A Raman study on the C(4)=O stretching mode of flavins in flavoenzymes: hydrogen bonding at the C(4)=O moiety. *J. Biochem.* **121**, 1147-1154
31. Wille, G., Ritter, M., Friedemann, R., Mantele, W., and Hubner, G. (2003) Redox-triggered FTIR difference spectra of FAD in aqueous solution and bound to flavoproteins. *Biochemistry* **42**, 14814-14821
32. Rüterjans, H., Fleischmann, G., Löhr, M., Knauf, F., Blümel, M., Lederer, F., Mayhew, S. G., and Müller, F. (1996) NMR Studies of Flavoproteins. *Biochem. Soc. Trans.* **24**, 116-121
33. Cui, D., Koder, R. L., Jr., Dutton, P. L., and Miller, A.-F. (2011) <sup>15</sup>N Solid-State NMR as a probe of Flavin H-bonding. *J. Phys. Chem. -B.* **115**, 7788-7798
34. Mohamed-Raseek, N., and Miller, A. F. (2022) Contrasting roles for two conserved arginines: stabilizing flavin semiquinone or quaternary structure, in bifurcating electron transfer flavoproteins. *J. Biol. Chem.* **298**, 101733
35. Dwyer, T. M., Zhang, L., Muller, M., Marrugo, F., and Frerman, F. E. (1999) The functions of the flavin contact residues  $\alpha$ Arg249 and  $\beta$ Tyr16, in human electron transfer flavoprotein. *Biochim. Biophys. Acta.* **1433(1-2)**, 139-152
36. Talfournier, F., Munro, A. W., Basran, J., Sutcliffe, M. J., Daff, S., Chapman, S. K., and Scrutton, N. S. (2001)  $\alpha$  Arg-237 in *Methylophilus methylotrophus* (sp. W3A1) electron-transferring flavoprotein affords approximately 200-millivolt stabilization of

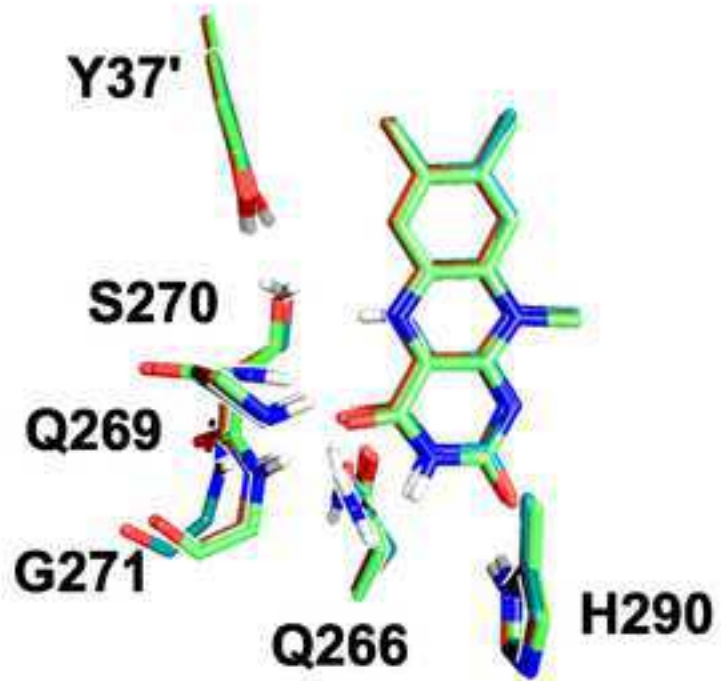
- the FAD anionic semiquinone and a kinetic block on full reduction to the dihydroquinone. *J Biol Chem* **276**, 20190-20196
- 1  
2  
3  
4  
5  
6  
7  
8  
9  
10  
11  
12  
13  
14  
15  
16  
17  
18  
19  
20  
21  
22  
23  
24  
25  
26  
27  
28  
29  
30  
31  
32  
33  
34  
35  
36  
37  
38  
39  
40  
41  
42  
43  
44  
45  
46  
47  
48  
49  
50  
51  
52  
53  
54  
55  
56  
57  
58  
59  
60  
61  
62  
63  
64  
65
37. Yang, K. Y., and Swenson, R. P. (2007) Modulation of the redox properties of the flavin cofactor through hydrogen-bonding interactions with the N(5) atom: Role of alpha Ser254 in the electron-transfer flavoprotein from the methylotrophic bacterium W3A1. *Biochem.* **46**, 2289-2297
38. Garcia Costas, A. M., Poudel, S., Miller, A.-F., J., S. G., Ledbetter, R. N., Fixen, K., Seefeldt, L. C., Adams, M. W., Harwood, C. S., Boyd, E. S., and Peters, J. W. (2017) Defining electron bifurcation in the electron transferring flavoprotein family. *J. Bacteriol.*
39. Chowdhury, N. P., Mowafy, A. M., Demmer, J. K., Upadhyay, V., Koelzer, S., Jayamani, E., Kahnt, J., Hornung, M., Demmer, U., Ermler, U., and Buckel, W. (2014) Studies on the mechanism of electron bifurcation catalyzed by electron transferring flavoprotein (Etf) and butyryl-CoA dehydrogenase (Bcd) of *Acidaminococcus fermentans*. *J. Biol. Chem.* **289**, 5145-5157
40. Morozenko, A., and Stuchebrukhov, A. A. (2016) Dowser++, a new method of hydrating protein structures. *Proteins, Structure Function Bioinformatics* **84**, 1347-1357
41. Case, D. A., Ben-Shalom, I. Y., Brozell, S. R., Cerutti, D. S., Cheatham, I., T.E., Cruzeiro, V. W. D., Darden, T. A., Duke, R. E., Ghoreishi, D., Gilson, M. K., Gohlke, H., Goetz, A. W., Greene, D., Harris, R., Homeyer, N., Huang, Y., Izadi, S., Kovalenko, A., Kurtzman, T., Lee, T. S., LeGrand, S., Li, P., Lin, C., Liu, J., Luchko, T., Luo, R., Mermelstein, D. J., Merz, K. M., Miao, Y., Monard, G., Nguyen, C., Nguyen, H., Omelyan, I., Onufriev, A., Pan, F., Qi, R., Roe, D. R., Roitberg, A., Sagui, C., Schott-Verdugo, S., Shen, J., Simmerling, C. L., Smith, J., SalomonFerrer, R., Swails, J., Walker, R. C., Wang, J., Wei, H., Wolf, R. M., Wu, X., Xiao, L., D.M., Y., and Kollman, P. A. (2018) AMBER 2018. University of California, San Francisco., San Francisco.
42. Tian, C., Kasavajhala, K., A., K. A., Belfon, K. A. A., Raguette, L., Huang, H., Miguez, A. N., Bickel, J., Wang, Y., Pincay, J., Wu, Q., and Simmerling, C. (2020) ff19SB: Amino-Acid-Specific Protein Backbone Parameters Trained against Quantum Mechanics Energy Surfaces in Solution. *J. Chem. Theory Comput.* **16**, 528-552
43. Wang, J., Wolf, R. M., Caldwell, J. W., Kollman, P. A., and Case, D. A. (2004) Development and testing of a general AMBER force field. *J. Comp. Chem.* **25**, 1157-1174
44. Wang, J., Wang, W., A., K. P., and Case, D. A. (2006) Automatic atom type and bond type perception in molecular mechanical calculations. *J. Mol. Graph. Model.* **25**, 247260
45. Bayly, C. I., Cieplak, P., Cornell, W., and Kollman, P. A. (1993) A well-behaved electrostatic potential based method using charge restraints for deriving atomic charges: the RESP model. *J. Phys. Chem* **97**, 10269-10280
46. Wei, B. Q., Weaver, L. H., Ferrari, A. M., Matthews, B. W., and Soichet, B. K. (2004) Testing a Flexible-receptor Docking Algorithm in a Model Binding Site. *J. Mol. Bio.* **337**, 1161-1182
47. Williams, C. J., Headd, J. J., Moriarty, N. W., Prisant, M. G., Videau, L. L., Deis, L. N., Verma, V., Keedy, D. A., Hintze, B. J., Chen, V. B., Jain, S., Lewis, S. M., Arendall, W. B., Snoeyink, J., Adams, P. D., Lovell, S. C., Richardson, J. S., and Richardson, D. C. (2017) MolProbity: More and better reference data for improved all-atom structure validation. *Prot. Sci.* **27**, 293-315
48. Neese, F., Wennmohs, F., Becker, U., and Riplinger, C. (2020) The ORCA quantum chemistry program package. *J. Chem. Phys.* **152**, 224108
49. Lu, Y., Farrow, M. R., Fayon, P., Logsdail, A. J., Sokol, A. A., Catlow, C. R. A., Sherwood, P., and Keal, T. W. (2019) Open-Source, Python-Based Redevelopment of the ChemShell Multiscale QM/MM Environment,. *J. Chem. Theory Comput.* **15**, 1317
50. Sherwood, P., de Vries, A. H., Guest, M. F., Schreckenbach, G., Catlow, C. R. A., French, S. A., Sokol, A. A., Bromley, S. T., Thiel, W., Turner, A. J., Billeter, S.,

- 1 Terstegen, F., Thiel, S., Kendrick, J., Rogers, S. C., Casci, J., Watson, M., King, F.,  
2 Karlsen, E., Sjøvoll, M., Fahmi, A., Schäfer, A., and Lennartz, C. (2003) QUASI: A  
3 general purpose implementation of the QM/MM approach and its application to  
4 problems in catalysis. *J. Mol. Str.: THEOCHEM* **632**, 1-28
- 5 51. Kästner, J., Carr, J. M., Keal, T. W., Thiel, W., Wander, A., and Sherwood, P. (2009)  
6 DL-FIND: An Open-Source Geometry Optimizer for Atomistic Simulations. *J. Phys.*  
7 *Chem. A* **113**, 11856-11865
- 8 52. Kulik, H. J., Luehr, N., Ufimtsev, I. S., and Martinez, T. J. (2012) Ab initio quantum  
9 chemistry for protein structures. *J. Phys. Chem. B* **116**, 12501-12509
- 10 53. Morozov, A. V., Kortemme, T., Tsemekhman, K., and Baker, D. (2004) Close  
11 agreement between the orientation dependence of hydrogen bonds observed in protein  
12 structures and quantum mechanical calculations. *Proc Natl Acad Sci U S A* **101**, 6946-  
13 6951
- 14 54. O'Meara, M. J., Leaver-Fay, A., Tyka, M. D., Stein, A., Houlihan, K., DiMaio, F.,  
15 Bradley, P., Kortemme, T., Baker, D., Snoeyink, J., and Kuhlman, B. (2015) Combined  
16 covalent-electrostatic model of hydrogen bonding improves structure prediction with  
17 rosetta. *J. Chem. Theory Comput.* **11**, 609-622
- 18 55. L.-P., W., J., C., and T., V. V. (2013) Systematic Parametrization of Polarizable Force  
19 Fields from Quantum Chemistry Data. *J. Chem. Theory Comput.* **9**, 452-460
- 20 56. Ponder, J., and Case, D. (2003) Force fields for protein simulations. *Adv. Protein Chem.*  
21 **66**, 27-65
- 22 57. Arunan, E., Desiraju, G. R., Klein, R. A., Sadlej, J., Scheiner, S., Alkorta, I., Clary, D.  
23 C., Crabtree, R. H., Dannenberg, J. J., Hobza, P., Kjaergaard, H. G., Legon, A. C.,  
24 Mennucci, B., and Nesbitt, D., J. (2011) Definition of the hydrogen bond (IUPAC  
25 Recommendations 2011). *Pure and Appl. Chem.* **83**, 1637-1641
- 26 58. Herschlag, D., and Pinney, M. M. (2018) Hydrogen bonds: Simple after all? *Biochem.*  
27 **57**, 3338-3352
- 28 59. Merski, M., Skrzeczkowski, J., Roth, J. K., and Górna, M. W. (2020) A geometric  
29 definition of short to medium range hydrogen-mediated interactions in proteins.  
30 *Molecules* **25**, 5326
- 31 60. Stranges, P. B., and Kuhlman, B. (2013) A comparison of successful and failed protein  
32 interface designs highlights the challenges of designing buried hydrogen bonds. *Prot.*  
33 *Sci.* **22**, 74-82
- 34 61. Tsujimura, M., and Ishikita, H. (2021) Identification of intermediate conformations in  
35 the photocycle of the light-driven sodium-pumping rhodopsin KR2. *J. Biol. Chem.* **296**,  
36 100459
- 37 62. Meng, E. C., Pettersen, E. F., Couch, G. S., Huang, C. C., and Ferrin, T. E. (2006)  
38 Tools for integrated sequence-structure analysis with UCSF Chimera. *BMC*  
39 *Bioinformatics* **7**, 339
- 40 63. Pettersen, E. F., Goddard, T. D., Huang, C. C., Couch, G. S., Greenblatt, D. M., Meng,  
41 E. C., and Ferrin, T. E. (2004) UCSF Chimera - a visualization system for exploratory  
42 research and analysis. *J. Comput. Chem.* **25**, 1605-1612
- 43 64. Sucharitakul, J., Buttranon, S., Wongnate, T., Chowdhury, N. P., Prongjit, M., Buckel,  
44 W., and Chaiyen, P. (2020) Modulations of the reduction potentials of flavin-based  
45 electron bifurcation complexes and semiquinone stabilities are key to control directional  
46 electron flow. *FEBS J. ASAP*, doi:10.1111/febs.15343
- 47 65. Ludwig, M. L., Pattridge, K. A., Metzger, A. L., Dixon, M. M., Eren, M., Feng, Y., and  
48 Swenson, R. P. (1997) Control of oxidation-reduction potentials in flavodoxin from  
49 *Clostridium beijerinckii*: the role of conformational changes. *Biochemistry* **36**, 1259-  
50 1280
- 51 66. Dwyer, T. M., Mortl, S., Kemter, K., Bacher, A., Fauq, A., and Frerman, F. E. (1999)  
52 The intraflavin hydrogen bond in human electron transfer flavoprotein modulates redox  
53 potentials and may participate in electron transfer. *Biochem* **38**, 9735-9745
- 54 67. Foster, J. P., and Weinhold, F. (1980) Natural Bond Orbitals. *J. Am. Chem. Soc.* **102**,  
55 7211
- 56  
57  
58  
59  
60  
61  
62  
63  
64  
65

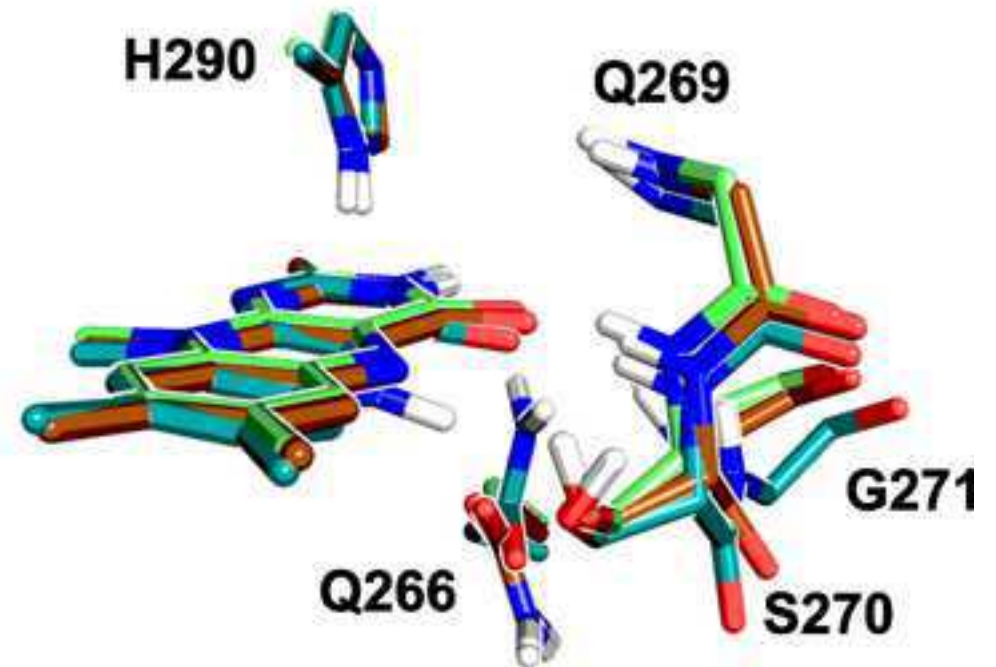
- 1  
2  
3  
4  
5  
6  
7  
8  
9  
10  
11  
12  
13  
14  
15  
16  
17  
18  
19  
20  
21  
22  
23  
24  
25  
26  
27  
28  
29  
30  
31  
32  
33  
34  
35  
36  
37  
38  
39  
40  
41  
42  
43  
44  
45  
46  
47  
48  
49  
50  
51  
52  
53  
54  
55  
56  
57  
58  
59  
60  
61  
62  
63  
64  
65
68. Zhang, Y.-L., Wang, F.-L., and Ren, A.-M. (2022) Reliability of computed molecular structures. *J. Comp. Chem.* **43**, 465-476
69. Unno, M., Masuda, S., Ono, T., and Yamauchi, S. (2006) Orientation of a key glutamine residue in the BLUF domain from AppA revealed by mutagenesis, spectroscopy, and quantum chemical calculations. *J. Am. Chem. Soc.* **128**, 5638-5639
70. Domratcheva, T., Hartmann, E., Schlichting, I., and Kottke, T. (2016) Evidence for tautomerisation of glutamine in BLUF blue light receptors by vibrational spectroscopy and computational chemistry. *Sci. Rep.* **6**, 22669
71. Wendler, K., Thar, J., Zahn, S., and Kirchner, B. (2010) Estimating the hydrogen bond energy. *J. Phys. Chem.* **114**, 9529-9536
72. Hall, L. H., Bowers, M. L., and Durfor, C. N. (1987) Further consideration of flavin coenzyme biochemistry afforded by geometry-optimized molecular orbital calculations. *Biochemistry* **26**, 7401-7409
73. Virgil, W., Jr., Tran, J., Niks, D., Schut, G. J., Ge, X., Adams, M. W. W., and Hille, R. (2022) The reductive half-reaction of two bifurcating electron-transferring flavoproteins: Evidence for changes in flavin reduction potentials mediated by specific conformational changes. *J. Biol. Chem.* **298**, 101927
74. Yikilmaz, E., Rodgers, D. W., and Miller, A.-F. (2006) The crucial importance of chemistry in the structure-function link: Manipulating hydrogen bonding in iron-containing superoxide dismutase. *Biochemistry* **45**, 1151-1161
75. Walsh, J. D., and Miller, A.-F. (2003) NMR Shieldings and Electron Correlation Reveal Remarkable Behaviour on the Part of the Flavin N<sub>5</sub> Reactive Center. *J. Phys. Chem. B* **107**, 854-863

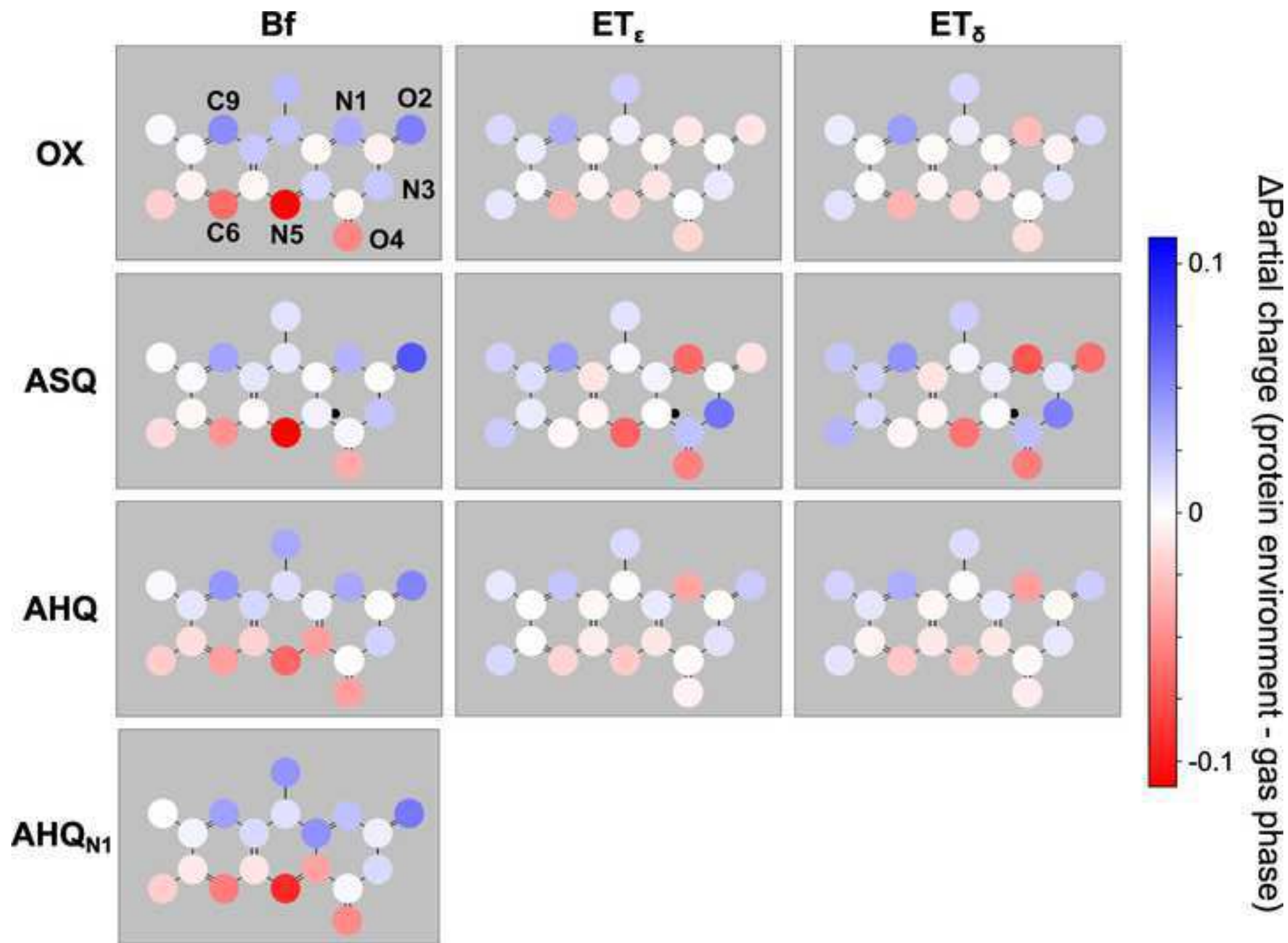


A

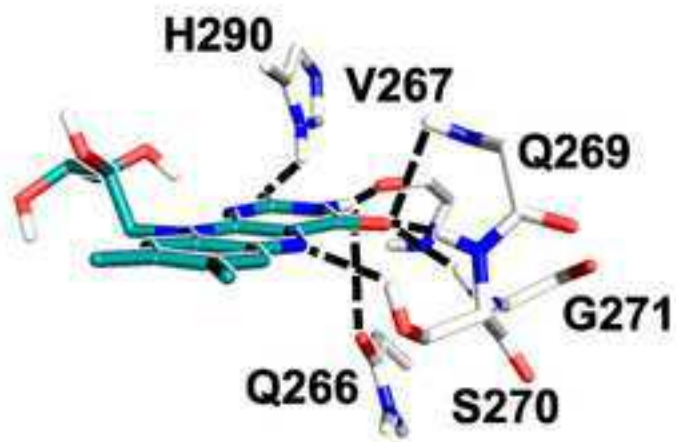
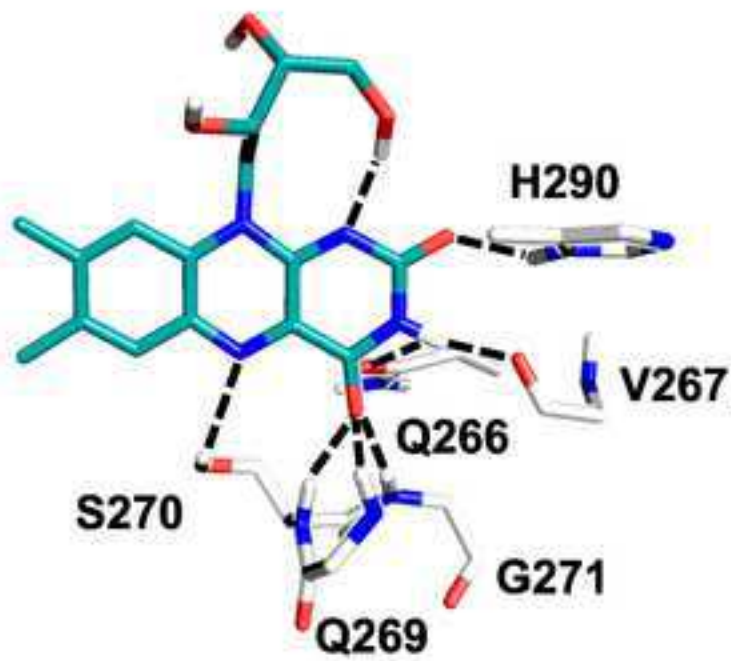


B

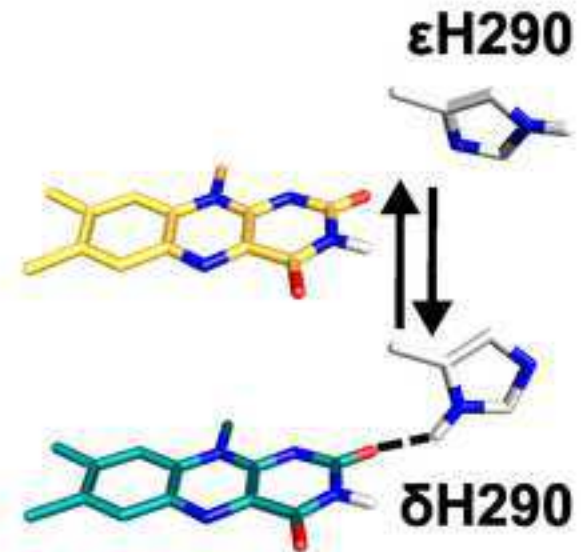




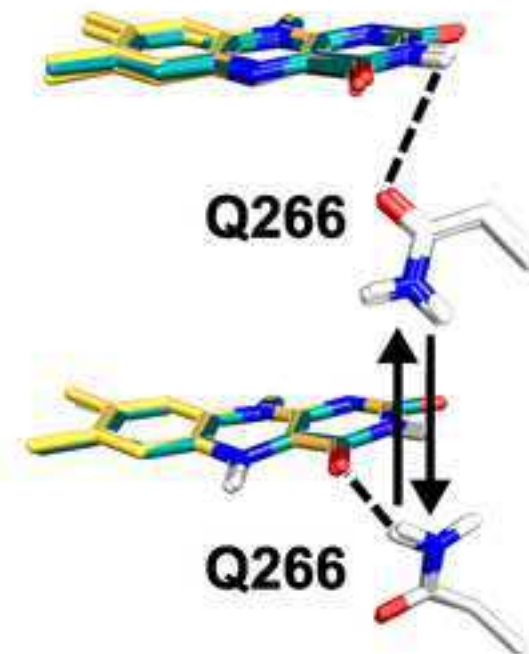
A



B



C

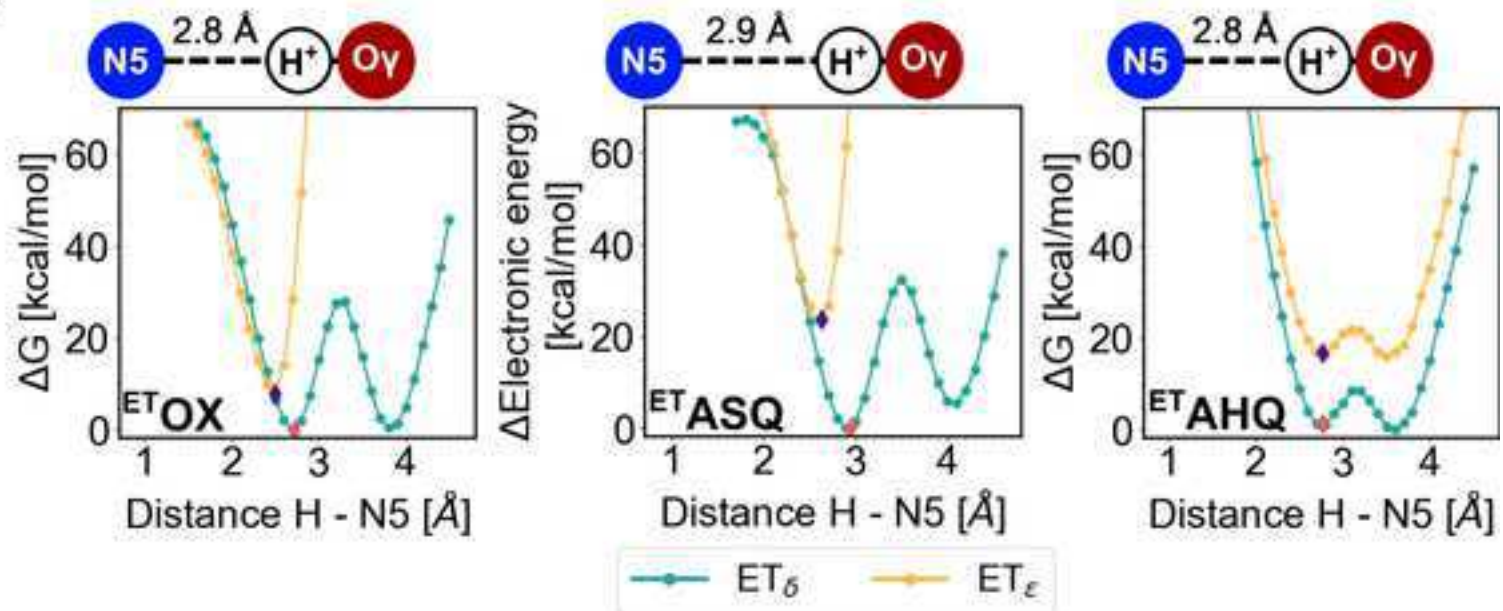




A

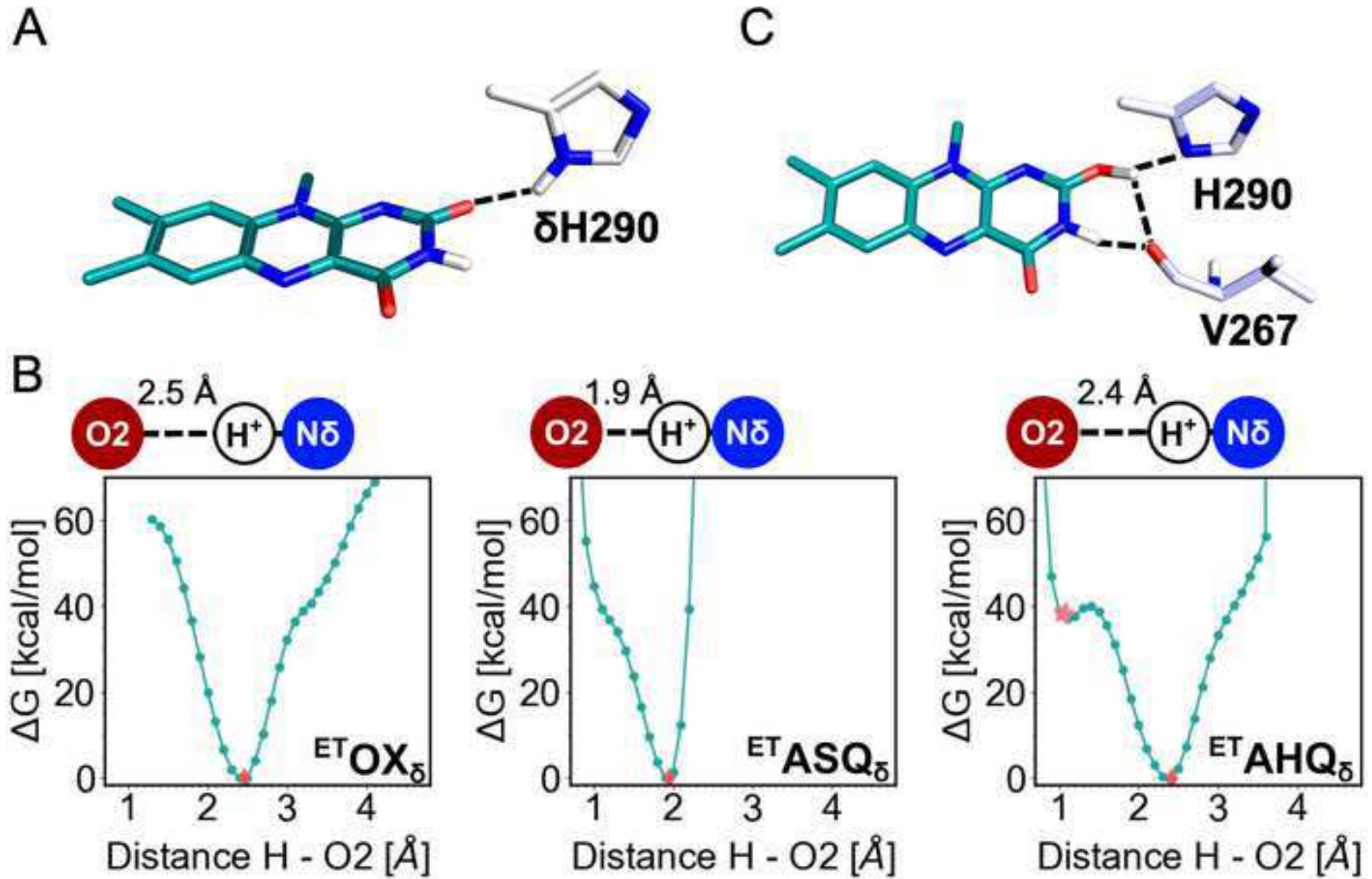


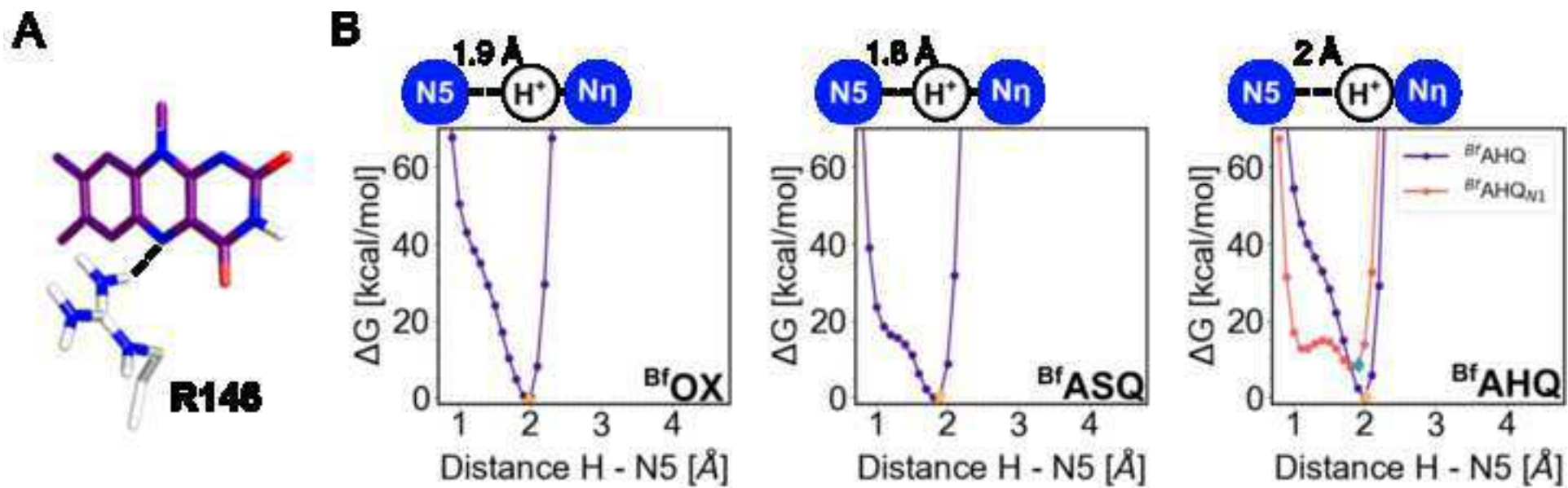
B



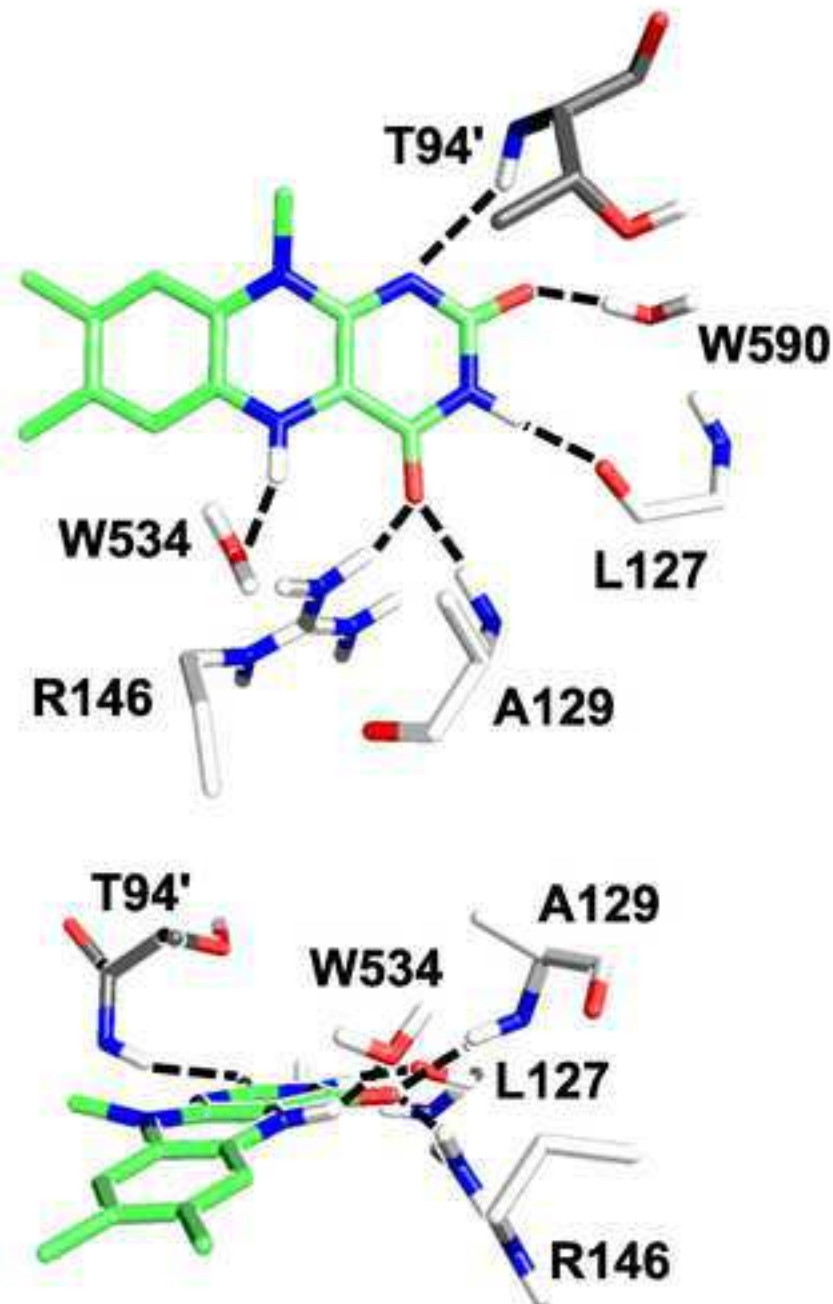
C



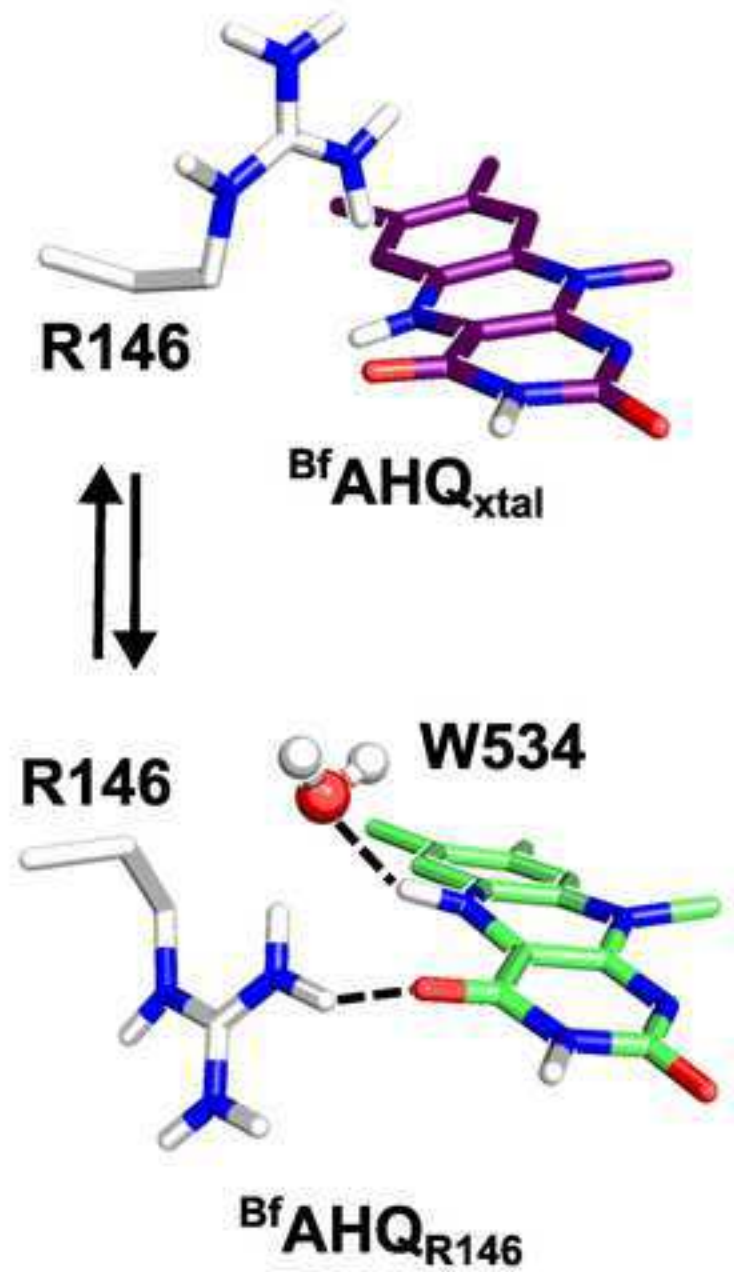


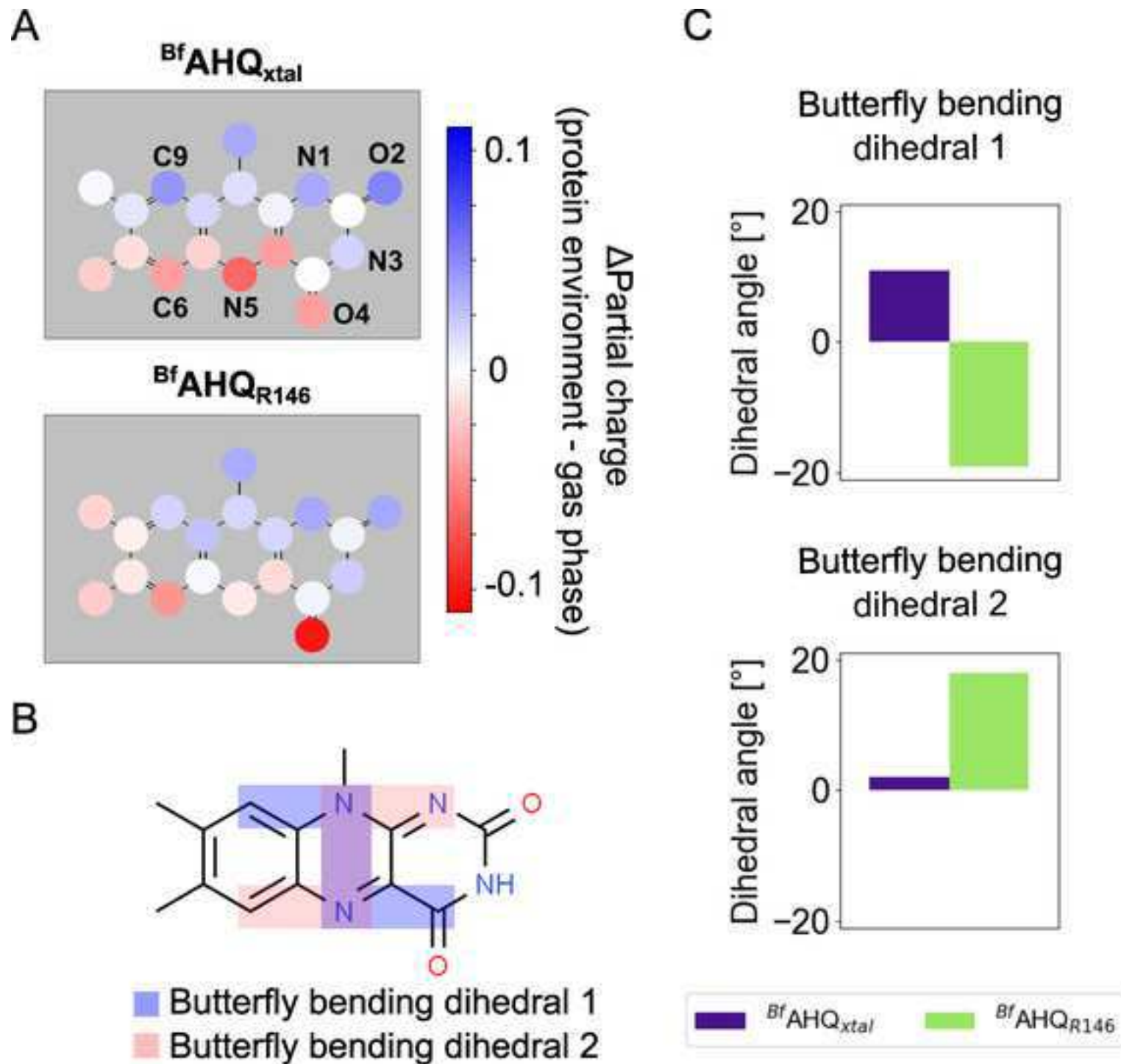


A

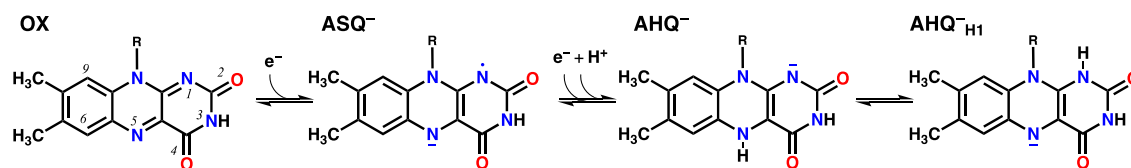


B





Scheme 1



Scheme 2

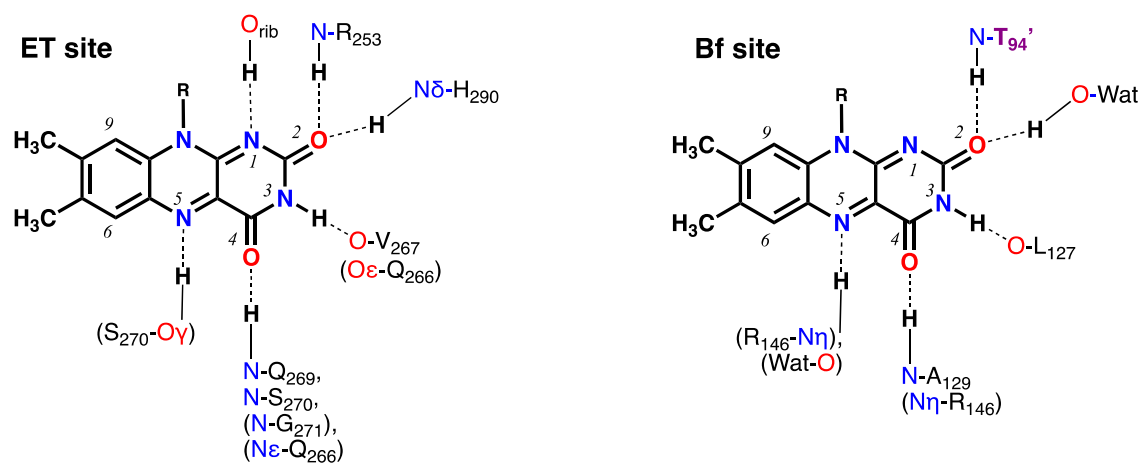


**Table 1:** Gibbs free energy differences between flavin oxidation states in each of the binding sites of *AfeETF*<sup>a, b</sup>

Flavin's environment	$\Delta G$ [kcal/mol]	
	ASQ - OX	AHQ - OX
Gas phase LF	-36	-408
<sup>Bf</sup> flavin	4	-352
<sup>ET</sup> flavin <sub><math>\delta</math></sub>	-73	-385
<sup>ET</sup> flavin <sub><math>\epsilon</math></sub>	-73	-388

<sup>a</sup> For the protein-bound flavins, the protein environment was represented as a distribution of electrostatic point charges. Comparisons can be made only within individual columns. The large difference between the sets of energies associated with each of the two chemical events may reflect our neglect of intrinsic energies of the electrons and proton that feature in the balanced equations for the different reductions.

<sup>b</sup> For completeness, corresponding electronic energy differences are given in SI Table S1.

**Table 2:** Models employed in this study<sup>a</sup>

<b>Name of the model</b>	<b>Description</b>
<sup>Bf</sup> OX	Bf flavin in oxidized state
<sup>Bf</sup> ASQ	Bf flavin in anionic semiquinone state
<sup>Bf</sup> AHQ	Bf flavin in anionic hydroquinone state
<sup>Bf</sup> AHQ <sub>H1</sub>	<sup>Bf</sup> AHQ protonated at <sup>Bf</sup> N1 instead of <sup>Bf</sup> N5
<sup>Bf</sup> AHQ <sub>R146</sub>	<sup>Bf</sup> AHQ with alternate rotamer of R146
<sup>ET</sup> OX <sub>ε</sub>	ET flavin in oxidized state, ε tautomer of H290
<sup>ET</sup> ASQ <sub>ε</sub>	ET flavin in anionic semiquinone state, ε tautomer of H290
<sup>ET</sup> AHQ <sub>ε</sub>	ET flavin in anionic hydroquinone state, ε tautomer of H290
<sup>ET</sup> OX <sub>δ</sub>	ET flavin in oxidized state, δ tautomer of H290
<sup>ET</sup> ASQ <sub>δ</sub>	ET flavin in anionic semiquinone state, δ tautomer of H290
<sup>ET</sup> AHQ <sub>δ</sub>	ET flavin in anionic hydroquinone state, δ tautomer of H290

<sup>a</sup>Structural formulae are provided in Scheme 1. The term 'flavin' is employed to refer specifically to the isoalloxazine head group of FAD, whereas FAD additionally includes adenosine diphosphate (ADP) ribose. A superscripted prefix is employed to specify which of the two flavins/FADs is intended. This notation is also applied to atoms within a flavin (see Schemes 1 and 2 for position numbering). OX refers to the oxidized state, ASQ to the anionic semiquinone, ASH to the anionic hydroquinone, NHQ to neutral hydroquinone, and when these occur alone they refer to the flavin, whereas 'FAD' is specified when the entire dinucleotide is intended. Residues from the EtfA chain are identified simply by their position number and one-letter code (e.g., R146), whereas residues from the EtfB chain are identified with an apostrophe (e.g., T94').